

# Does the fine-structure constant vary with cosmological epoch?

John N. Bahcall

*Institute for Advanced Study, Olden Lane, Princeton, NJ 08540*

Charles L. Steinhardt and David Schlegel

*Department of Astrophysical Sciences, Princeton University, Princeton, NJ 08544*

## ABSTRACT

We use the strong nebular emission lines of O III, 5007 Å and 4959 Å, to set a robust upper limit on the time dependence of the fine structure constant. We find  $|\alpha^{-1}d\alpha(t)/dt| < 10^{-13} \text{ yr}^{-1}$ , corresponding to  $\Delta\alpha/\alpha(0) = (-2 \pm 1.2) \times 10^{-4}$  for quasars with  $0.16 < z < 0.80$  obtained from the SDSS Early Data Release. Using a blind analysis, we show that the upper limit given here is invariant with respect to 17 different ways of selecting the sample and analyzing the data. As a by-product, we show that the ratio of transition probabilities corresponding to the 5007 Å and 4959 Å lines is  $3.01 \pm 0.02$ , in good agreement with (but more accurate than) theoretical estimates. We compare and contrast the O III emission line method used here with the Many-Multiplet method that was used recently to suggest evidence for a time-dependent  $\alpha$ .

*Subject headings:* atomic data; line: identification; line: profiles; quasars: absorption lines; quasars: emission lines

## 1. Introduction

We develop in this paper a robust analysis strategy for using the fine-structure splitting of the O III emission lines of distant quasars or galaxies to test whether the fine-structure constant,  $\alpha$ , depends upon cosmic time. We concentrate here on the two strongest nebular emission lines of O III, 5007 Å and 4959 Å, which were first used for this purpose by Bahcall & Salpeter (1965).

We begin this introduction with a brief history of astronomical studies of the time dependence of the fine structure constant (§ 1.1) and then describe some of the relative advantages of using either absorption lines or emission lines for this purpose (§ 1.2). Next, we provide an outline of the paper (§ 1.3). Finally, since some of the material in this paper is intended for experts, we provide suggestions as to how the paper should be read, or not read (§ 1.4).

We limit ourselves in this paper to tests in which  $\alpha$  is the only dimensionless fundamental constant whose time dependence can affect the measurements in any significant way.

### 1.1. A brief history

Savedoff (1956) set the first astronomical upper limit on the time dependence of  $\alpha$  using the fine-structure splitting of emission lines of N II and Ne III in the spectrum of the nearby radio galaxy Cygnus A. He reported  $\alpha^2(z = 0.057)/\alpha^2(0) = 1.0036 \pm 0.003$ . This technique was first applied to distant quasar spectra by Bahcall & Salpeter (1965), who used emission lines of O III and Ne III in the spectra of 3C 47 and 3C 147 to set an upper limit of  $|\alpha^{-1}d\alpha(t)/dt| < 10^{-12} \text{ yr}^{-1}$ . Bahcall & Schmidt (1967) obtained a similar limit,  $< 10^{-12} \text{ yr}^{-1}$ , using the O III emission lines in five radio galaxies. Here, and elsewhere in the paper, we shall compare limits on the time-dependence of  $\alpha$  obtained at different cosmic epochs by assuming  $\alpha$  depends linearly on cosmic time for redshifts less than five. The assumption of linearity may misrepresent the actual time dependence, if any, but it provides a simple way of comparing measurements at different redshifts.

The technique of using emission lines to investigate the time dependence of  $\alpha$  was abandoned after 1967. In this sense, the present paper is an attempt to push the frontiers of the subject backwards three and a half decades.

Bahcall, Sargent, & Schmidt (1967) first used quasar absorption (not emission) lines to investigate the time dependence of  $\alpha$ . They used the doublet fine-structure splitting of Si II and Si IV absorption lines in the spectrum of the bright radio quasar 3C 191,  $z = 1.95$ . Although the results referred to a relatively large redshift, the precision obtained,  $\alpha(z = 1.95)/\alpha(0) = 0.98 \pm 0.05$ , corresponding to  $|\alpha^{-1}d\alpha(t)/dt| < 7 \times 10^{-12} \text{ yr}^{-1}$ , did not represent an improvement.

Since 1967, there have been many important studies of the cosmic time-dependence of  $\alpha$  using quasar absorption lines. Some of the most comprehensive and detailed investigations are described in papers by Wolfe, Brown, & Roberts (1976), Levshakov (1994), Potekhin & Varshalovich (1994), Cowie & Songaila (1995), and Ivanchik, Potekhin, & Varshalovich (1999). The results reported in all of these papers are consistent with a fine-structure constant that does not vary with cosmological epoch.

Recently, the subject has become of great interest for both physicists and astronomers because of the suggestion that a significant time-dependence has been found using absorption lines from many different multiplets in different ions, the ‘Many-Multiplet’ method (see, e.g., the important papers by Dzuba, Flambaum, & Webb 1999a,b; Webb et al. 1999; Murphy et al. 2001a,b; and Webb et al. 2002). The suggestion that  $\alpha$  may be time dependent is particularly of interest to physicists in connection with the possibility that time-dependent coupling constants may be related to large extra dimensions (see Marciano 1984). Unlike the previous emission line or absorption line studies, the Many-Multiplet collaboration uses absolute wavelengths rather than the ratio of fine-structure splittings to average wavelengths. We shall compare and contrast in § 8 the emission line technique used here with the Many-Multiplet method.

## 1.2. Absorption versus emission lines

Why have absorption line studies of the time-dependence of  $\alpha$  dominated over emission line studies in the last three and a half years? There are two principal reasons that absorption lines have been preferred. First, the resonant atomic absorption lines can be observed at large redshifts since their rest wavelengths fall in the ultraviolet. By contrast, emission line studies are limited to smaller redshifts ( $z < 1.5$ ) since the most useful emission lines are in the visual region of the spectrum. Second, there are many absorption lines, often hundreds, observed in the spectra of large redshift quasars and galaxies. These lines are produced by gas clouds at many different redshifts. There is only one set of emission lines with one redshift, representing the cosmic distance of the source from us, for each quasar or galaxy.

Why have we chosen to return to quasar emission lines as a tool for studying the time dependence of  $\alpha$ ? We shall show that emission lines can be used to make precision measurements of the time dependence of  $\alpha$  while avoiding some of the complications and systematic uncertainties that affect absorption line measurements. In addition, the large sample of distant objects made available by modern redshift surveys like the SDSS survey (Stoughton et al. 2002; Schneider et al. 2002) and the 2dF survey (Boyle et al. 2000; Croom et al. 2001) provide large samples of high signal-to-noise spectra of distant objects.

In this paper, we select algorithmically, from among 3814 quasar spectra in the SDSS Early Data Release (EDR, Schneider et al. 2002), the quasar spectra containing O III emission lines that are most suitable for precision measurements. A total of 107 quasar spectra pass at least 3 out of the 4 selection tests we impose on our standard sample in § 5. Our Standard Sample contains spectra of 44 quasars. We also study alternative samples obtained using variants of our standard selection algorithm. These alternative samples contain between 29 and 73 individual quasar spectra.

The techniques described in this paper could be applied to similar transitions in [Ne III] ( $\lambda\lambda 3968, 3869$ ) and in [Ne V] ( $\lambda\lambda 3426, 3346$ ). However, the [O III] emission lines are typically an order of magnitude stronger in quasar spectra than the just-mentioned transitions of [Ne III] and [Ne V] (cf. Vanden Berk et al 2001; Schneider et al. 2002). Moreover, the intensity ratio of the [O III] lines is a convenient value (about 3.0) and the relevant region of the spectrum is relatively free of other possibly contaminating emission or absorption lines. After [O III], the [Ne III] lines are the most promising pair of emission lines for studies of the time dependence of  $\alpha$ .

## 1.3. Outline of the paper

We present in § 2 a summary of the main ingredients in the analysis we perform. Then in § 3 we describe how we developed the selection algorithm and performed the analysis blindly, i.e., without knowing what the results meant quantitatively until all of the measurements and calculations were complete. We present in § 4 the key procedure which we have used to measure by how many

Angstroms we have to shift the observed 4959 Å line profile to obtain a best-fit match to the 5007 Å line profile.

The Standard Sample of quasar spectra that we measure is selected objectively by applying four computer tests designed to ensure that emission line pairs that are used in the analysis will yield accurate and unbiased estimates of  $\alpha$ . These selection tests are described in § 5. Figure 3 illustrates a good quasar spectrum that easily passes all of the computer tests. Figure 4 shows four spectra, each of which illustrates a failure to satisfy one of the four standard tests.

Table 1 and Table 2, together with Figure 6, present our principal results. The results for our Standard Sample are explained in § 6, where we discuss the average value of  $\alpha$  and the best-fit slope,  $d\alpha(t)/dt$ , for our Standard Sample of 44 quasars. We also describe in this section the bootstrap method that we have used to calculate the uncertainties for the sample characteristics. In § 7, we describe and discuss the analysis of 17 additional samples chosen by alternative selection algorithms. We describe the ‘Many-Multiplet’ method in § 8 and contrast the O III method with the Many-Multiplet method. We summarize and discuss our results in § 9.

#### 1.4. How should this paper be read?

This paper contains many different things, including (not necessarily in this order): 1) a detailed discussion of the algorithmic basis for selecting the 18 different samples that we analyze, 2) a description of how our algorithmic measurements are made in practice, 3) a discussion of the errors in the measurements, 4) tabulated details of the measurements sufficient to allow the reader to change or check the data analysis, 5) quantitative results on the time dependence of the fine structure constant in our Standard Sample, 6) quantitative results on the time dependence of  $\alpha$  for 17 alternative samples, 7) a comparison of the Many-Multiplet and O III methods for studying the time dependence of the fine structure, and 8) a summary and discussion of our main conclusions. In addition, we present an accurate measurement of the ratio of the two forbidden transition probabilities that lead to the 5007 Å and 4959 Å lines.

Most readers will only want to sample part of this fare. Here is our suggestion as to how to get the most out of the paper in the shortest amount of time. We assume that you have read the introduction. If so, then you probably will want to first read § 2, which gives an outline of the procedure we follow, and then look at Figure 1, Figure 3, and Figure 6. Next read the conclusions and discussion in § 9. If you are especially interested in the differences between the O III method and the Many-Multiplet method, then look at Table 3 and, if you want more details about the differences, read § 8. Our principal quantitative results are given in § 6 and § 7. Unless you are an expert, you can skip everything in § 6 and § 7 except the simple equations that give the main numerical results: Eq. (17)–Eq. (23). Sections 3–5 contain the main technical discussion of this paper. These sections are essential for the expert who wants to decide whether we have done a good job. But, if you have already made up your mind on this question, you can skip §§ 3–5.

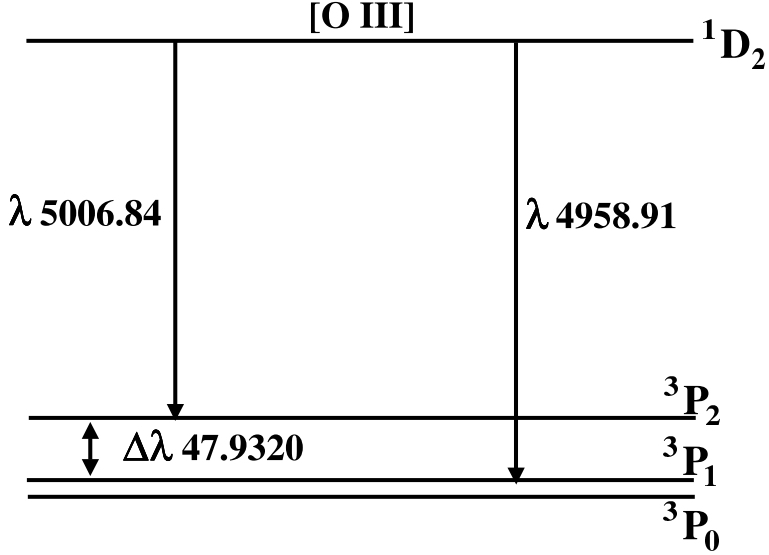


Fig. 1.— Energy level diagram for O III. The figure shows the two strong emission lines that arise from the same  $^1D_2$  excited level of twice-ionized oxygen. The 5007 Å and 4959 Å lines are separated by about 48 Å by the fine-structure energies of the ground-state triplet P states. The wavelength separation  $\Delta\lambda$  divided by the sum of the wavelengths of the two emission lines is proportional to  $\alpha^2$ ; this dimensionless ratio (difference divided by sum) is defined as  $R$  in Eq. (1). The quantity  $R$  can be measured in distant quasars or galaxies and is independent of cosmological epoch unless  $\alpha^2$  depends upon time.

## 2. Outline of measurement procedure

Figure 1 shows the relevant part of the energy level diagram for twice-ionized oxygen, O III. We utilize in this paper the two strongest nebular emission lines of [O III],  $\lambda 5007$  and  $\lambda 4959$ , both of which originate on the same initial excited level,  $^1D_2$ . Since both lines originate on the same energy level and both lines have a negligible optical depth (the transitions are strongly forbidden), both lines have exactly the same emission line profile<sup>1</sup>. If there are multiple clouds that contribute to the observed emission line, then the observed emission line profiles are composed of the same mixture of individual cloud complexes.

The two final states are separated by the fine-structure interaction. Thus the energy separation of the  $\lambda 5007$  and  $\lambda 4959$  emission lines is proportional to  $\alpha^4$ , while the leading term in the energy separation for each line is proportional to  $\alpha^2$ . To very high accuracy (see § A of the Appendix,),

---

<sup>1</sup>The effect of differential reddening on the line splitting can easily be shown to be  $\sim 10^{-8}\tau_0$ , where  $\tau_0$  is the optical depth at 5007 Å. This shift is negligible, more than four orders of magnitude less than our measurement uncertainties.

the difference in the wavelengths divided by the average of the wavelengths,  $R$ ,

$$R(t) = \frac{\lambda_2(t) - \lambda_1(t)}{\lambda_1(t) + \lambda_2(t)}, \quad (1)$$

is proportional to  $\alpha^2$ . The cosmological redshift of the astronomical source that emitted the oxygen lines cancels out of the expression for  $R$ , which depends only on the ratio of measured wavelengths, either added or subtracted. Thus a measurement of  $R$  is a measurement of  $\alpha^2$  at the epoch at which the [O III] lines are emitted. The key element in measuring  $R(t)$  is the determination of the shift in Angstroms that produces the best-fit between the line profiles of the two emission lines.

The wavelengths in air of the nebular emission lines

$$\lambda_1 = 4958.9110 \text{ \AA}; \quad \lambda_2 = 5006.8430 \text{ \AA}, \quad (2)$$

and their separation

$$\Delta\lambda = 47.9320 \text{ \AA}, \quad (3)$$

have been measured accurately from a combination of laboratory measurements with a theta-pinch discharge (Pettersson 1982) and, for the wavelength separation, infrared spectroscopy with a balloon borne Michelson interferometer (Moorwood et al. 1980). The conversion from vacuum wavelengths to wavelengths in air was made using the three term formula of Peck and Reeder (1972). Combining Eq. (2) and Eq. (3), we have

$$R(0) = 4.80967 \times 10^{-3} [1 \pm 0.00001], \quad (4)$$

where the error for  $R(0)$  is based primarily on measurement by Moorwood et al. (1980) of the intervals in the ground  $^3P$  multiplet (see also Pettersson 1982).

One can write the ratio of  $\alpha^2$  at much earlier time  $t$  to the value of  $\alpha^2$  obtaining at the current cosmological epoch as

$$\frac{R(t)}{R(0)} = \frac{\alpha^2(t)}{\alpha^2(0)} = \left[ \frac{\Delta\lambda(t)}{\lambda_1(t) + \lambda_2(t)} \right] \left[ \frac{\lambda_1(0) + \lambda_2(0)}{\Delta\lambda(0)} \right]. \quad (5)$$

The light we observe today was emitted by distant quasars (or galaxies) at an epoch that was  $10^9$  yr or  $10^{10}$  yr earlier. This huge time difference makes possible precise measurements of the time dependence of  $\alpha^2$  by recording the redshifted wavelengths of the [O III] emission lines emitted at a much earlier epoch.

We will compare values of  $R$ , i.e.,  $\alpha^2$ , measured at different cosmological epochs. Although the data are consistent with a time-independent value for  $\alpha^2$ , we will find an upper limit to the possible time-dependence by fitting the measured values of  $R(t)$  to a linear function of time,

$$R(t) = R(0)[1 + StH_0]. \quad (6)$$

Here  $R(t)$  is a function of  $z$ ,  $R(t(z))$ , where  $z$  is the cosmological redshift [see Eq. (8)] below for the relation between  $t$  and  $z$ ). The slope  $S$  is twice the logarithmic derivative of  $\alpha^2(t)$  with respect to time in units of one over the Hubble constant.

$$S = \frac{1}{H_0 \alpha^2} \left( \frac{d\alpha^2}{dt} \right) = \frac{2}{H_0 \alpha} \left( \frac{d\alpha}{dt} \right) \quad (7)$$

As defined in Eq. (6) and Eq. (7), the slope  $S$  is independent of  $H_0$ . Each redshift produces a unique value of  $H_0 t$ .

We do not need to know  $\alpha^2(0)$ , or equivalently,  $\lambda_1$  and  $\lambda_2$  (or  $R(0)$ ), in order to test for the time dependence of  $\alpha$ . We can use Eq. (5) and Eq. (6) to explore the time dependence by simply taking  $\alpha^2(0)$  to be any convenient constant. In fact, this is exactly what we have done, which enabled us to carry out a blind analysis (see discussion in § 3). For 16 of the 17 samples we have analyzed, we have not made use of the known local value for  $R(0)$ , i.e.,  $\alpha^2(0)$  (see § 7).

The cosmological time can be evaluated from the well known expression (e.g., Carroll and Press 1992)

$$t = \frac{t_0 - t_1}{H_0} = \int_0^z \frac{dz}{(1+z)\sqrt{(1+z)(1+\Omega_m z) - z(2+z)\Omega_\Lambda}}, \quad (8)$$

where  $\Omega_m$  and  $\Omega_\Lambda$  are the usual present-epoch fractional contributions of matter and a cosmological constant to the cosmological expansion. The translation between the Hubble constant,  $H_0$ , and a year is given by

$$\frac{1}{H_0} = 1.358 \times 10^{10} \text{ yr}^{-1} \left( \frac{72 \text{ km s}^{-1} \text{Mpc}^{-1}}{H_0} \right). \quad (9)$$

In what follows, we shall adopt the value for  $H_0$  determined by the HST Key Project, i.e.,  $H_0 = 72 \text{ km s}^{-1} \text{Mpc}^{-1}$  (Freedman et al. 2001). If the reader prefers a different value for  $H_0$ , all times given in this paper can be rescaled using Eq. (9). Except where explicitly stated otherwise in the remainder of the paper, the time  $t$  is calculated from Eq. (8) and Eq. (9) for a universe with the present composition of  $\Omega_m = 0.3$ ,  $\Omega_\Lambda = 0.7$ .

### 3. Blind analysis

To avoid biases, we performed a blind analysis.

Measurements of  $\alpha^2$  were computed relative to an artificial value of  $\alpha^2(0)_{\text{artificial}} = 1.0$ . We did not renormalize the measured values of  $\alpha^2(t)$  until the analysis was complete. In fact, we did not search out the precise values of the wavelengths given in Eq. (2) until after we had finished all our calculations of  $\alpha^2(t)$  from the measured wavelengths. Throughout all the stages when we were determining the selection criteria for the sample described in § 5, we worked with measured values for  $\alpha^2(t)$  that were about 0.0048 [cf. Eq. (4)]. At this stage, we had not researched the precise values of the local wavelengths for the [O III] emission lines. Therefore, we did not know whether

the measured values that we were getting for  $\alpha^2(t)$  were close to the local value and, if so, how close.

To further separate the measuring process from any knowledge of the local value for  $\alpha(0)$ , we developed the criteria for selecting the sample using a subset of the quasars in the SDSS EDR sample. We used in this initial sample 313 quasars with redshifts  $z < 0.80$ . After finalizing the selection criteria, we applied the criteria to the remaining 389 quasars with  $z < 0.80$  in the EDR. The acceptance rate for the initial sample was 24 objects out of 313 or 7.7%, while the acceptance rate for the second sample was 20 out of 389 or 5.1%. We will refer later to the combined sample of 44 objects selected in this way as our ‘standard sample.’

The estimates of  $\alpha^2$  derived for the two parts of the standard sample were in excellent agreement with each other. For the initial sample of 24 objects, we found

$$\langle \alpha^2 \rangle = 0.9995 \pm 0.0002, \quad (10)$$

and for the second sample of 20 objects we found

$$\langle \alpha^2 \rangle = 0.9996 \pm 0.0005. \quad (11)$$

The sample average for the 44 objects is  $0.9996 \pm 0.0002$  (cf. row one of Table 1 in § 6).

#### 4. Matching the 5007 Å and 4959 Å line shapes

The key element in our measurement of  $\alpha$  is the procedure by which we match the shapes of the 5007 Å and 4959 Å emission line profiles. What we want to know is by how many Angstroms do we have to shift the 4959 Å line so that it best fits the measured profile of the 5007 Å line. In the process, we also determine a best-estimate for the ratio of the intensities in the two lines.

Figure 1 shows that both of the emission lines, [O III] 5007 Å and 4959 Å, arise from the same initial atomic state. Hence both lines have (within the accuracy of the noise in the measurements) the same line profile, i.e., the same shape of the curve showing the flux intensity versus wavelength, although the two lines are displaced in wavelength and have different intensities.

We have developed a computer code, FitAlpha, that finds the best match of the shapes of the 5007 Å and 4959 Å lines in terms of two parameters,  $\eta$  and  $A$ . The two parameters describe how much the measured profile of the 4959 Å line must be shifted in wavelength,  $\eta$ , and how much the 4959 Å profile must be increased in amplitude,  $A$ , in order to provide the best possible match to the profile of the 5007 Å emission line.

We first discuss in § 4.1 the measurements of the amplitude ratios  $A$  and then describe in § 4.2 the measurements of the quantity that describes the wavelength shift,  $\eta$ . We conclude by describing in § 4.3 the errors that we assign to individual measurements of  $\alpha^2$ .

#### 4.1. Amplitude ratios A

In the limit in which the profiles of the 5007 Å and 4959 Å lines match identically and there is no measurement noise, the quantity  $A$  is the ratio of the area under the 5007 Å line to the area under the 4959 Å line. More explicitly, in the limit of an ideal match of the two line profiles,

$$A = \frac{\int_{5007} [\text{LineFlux}(\lambda) - \text{ContinuumFlux}(\lambda)] d\lambda}{\int_{4959} [\text{LineFlux}(\lambda) - \text{ContinuumFlux}(\lambda)] d\lambda}. \quad (12)$$

In practice, the best-fit ratio of the amplitudes, which is measured by FitAlpha, is better determined than the area under the emission lines. Thus, the values we report for  $A$  (e.g. in Table 4 in § B of the Appendix) are the best-fit ratios of the amplitudes. Although  $A$  is one of the outputs of FitAlpha, we do not make use of  $A$  except as a *post facto* sanity check that the fits are sensible.

Figure 2 presents a histogram of the values of  $A$  that were measured for quasars in our standard sample, which is defined in § 5. Our measurements have a typical  $1\sigma$  spread of about  $\pm 0.1$ . The sample average of the measurements for  $A$ , and the bootstrap uncertainty determined as described in § 6.2, are

$$\langle A_{\text{measured}} \rangle = 3.01 \pm 0.02. \quad (13)$$

The quantity  $\langle A_{\text{measured}} \rangle$  is equal to the ratio of the decay rates of the 5007 Å and the 4959 Å lines, i.e., the ratio of the Einstein  $A$  coefficients. Thus the measured value for the ratio of the transition probabilities corresponding to the 5007 Å and 4959 Å lines is

$$\frac{A(5007)}{A(4959)} = 3.01 \pm 0.02. \quad (14)$$

The measured value of  $A(5007)/A(4959)$  is consistent with the best theoretical estimate given in the NIST Atomic Spectra Database,  $A(5007)/A(4959) = 2.92$  (Wiese, Fuhr, and Deter 1996). The quoted NIST accuracy level for this theoretical estimate is ‘B’, which generally corresponds to a numerical accuracy of better than 10%. Our measurement is more accurate than the theoretical estimate.

#### 4.2. Measuring $\eta$ and $R$

We define  $\eta$  by the relation

$$\eta \equiv \frac{\lambda_2}{\lambda_1} - 1, \quad (15)$$

where  $\lambda_1$  and  $\lambda_2$  are the measured values of the redshifted emission lines corresponding to the lines with rest wavelengths given by Eq. (2). We use the measured values of  $\eta$  to calculate the value of  $\alpha^2(z)$  for each source. The ratio  $R$  defined by Eq. (1) can be written in terms of  $\eta$  as

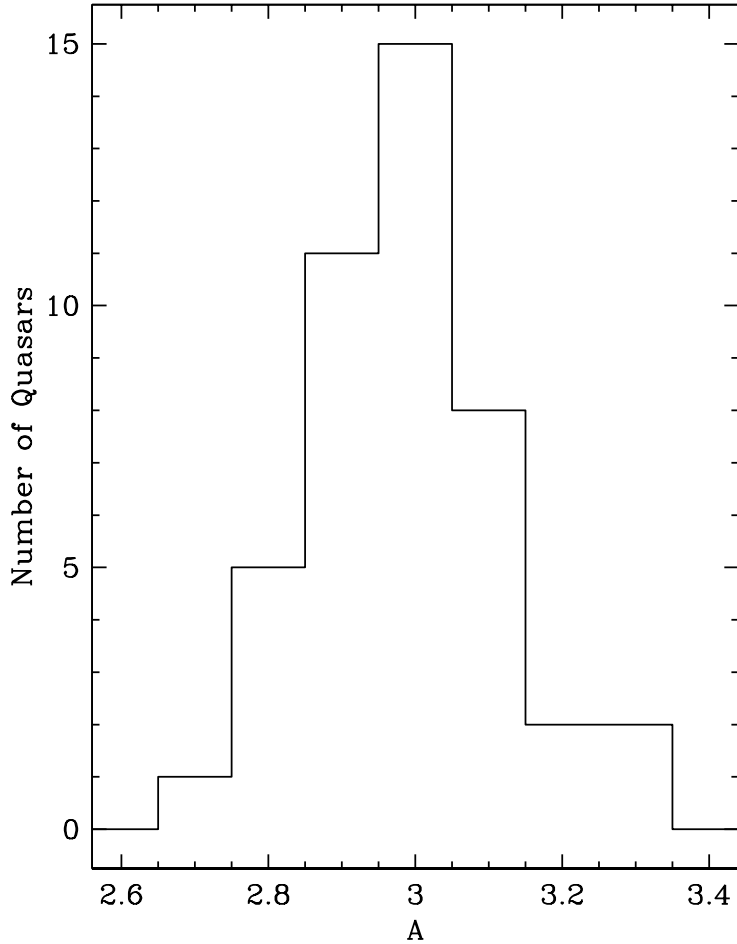


Fig. 2.— The ratio of amplitudes,  $A$ . The figure shows a histogram for our standard sample of quasars of the ratio  $A$ , which is the best-fit ratio of the amplitude of the 5007 Å profile to the amplitude of the 4959 Å profile. The measured average value of  $A$  is in good agreement with the expectation based upon the tabulated data in the NIST Atomic Spectra Database (see Eq. 13 and Eq. 14 and related text.)

$$R = \frac{\eta}{\eta + 2}. \quad (16)$$

FitAlpha finds the best-fit values of  $\eta$  as follows. The Princeton 1-D reduction code (Schlegel 2003) determines the redshift of the quasar by fitting the entire quasar spectrum to a template. This fit yields an approximate value for the redshift that locates the 4959 Å and 5007 Å lines to within 2-3 spectral pixels. Each of the spline-resampled pixels has a width of  $69.0 \text{ km s}^{-1}$ . FitAlpha selects a 20 pixel wide region of the spectrum centered around the expected center of the 4959 Å line and a wider (35 pixel) region around the expected center of the 5007 Å line. The Spectro-2D code

represents each quasar spectrum as a 4<sup>th</sup> order B-spline, where the spline points are spaced linearly in log-wavelength (Burles and Schlegel 2003),  $\log \lambda_1 = \text{const.} + 10^{-4} \times i$ . The optical output of the SDSS spectrograph gives pixel elements that are very nearly proportional to  $\log \lambda$ . This B-spline can be evaluated at any choice of wavelengths. We chose to evaluate each spectrum on a dense grid spaced in units of  $10^{-5}$  in log-wavelength ( $\sim 0.1$  pixel), corresponding to approximately  $6.9 \text{ km s}^{-1}$ . The measured average full width at half maximum of the 5007 Å lines in our standard sample is 5.5 pixels ( $\sim 9 \text{ \AA}$ ).

The measured profile of the 4959 Å line is compared with each of the spline-fit representations of the 5007 Å region. We make the comparison only within a region of  $2 \times 10^{-3}$  in log-wavelength (about 23 Å). For each possible shift between the two emission lines in log-wavelength, we minimize over the multiplicative scale factor  $A$  between the profiles of the two lines and a quadratic representation of the local continuum. This continuum is primarily the approximately power-law of the quasar spectrum and the wings of the H $\beta$  line. The value of  $\eta$  (cf. Eq. 15) is determined by minimizing the  $\chi^2$  value for the fit between the two line shapes.

#### 4.3. Error estimates on individual measurements

The errors on the measured SDSS fluxes are not perfectly correct; the pipeline software over-estimates the errors for lower flux levels. We correct the errors approximately by multiplying all of the errors by a constant factor (typically of order 0.75) chosen to make  $\chi^2$  per degree of freedom equal to 1 for the best-fit value of  $\eta$ . These adjusted errors are used to evaluate the uncertainty in the measured value of  $\eta$ . However, we show in § 6 and in § 7.2.4 that the bootstrap error for the sample average value of  $\alpha$  and of the first derivative of  $\alpha$  with time are very insensitive to the estimated uncertainties in the individual measurements.

The error on the measured value of  $\alpha^2$  is dominated by the error on the measurement of the wavelength separation,  $\Delta\lambda$ , between the 5007 Å and the 4959 Å line. Before making the measurements, we estimated, based upon prior experience with CCD spectra, that we should be able to measure  $\Delta\lambda$  to about 0.05 of a pixel. Since the width of each pixel is about  $70 \text{ km s}^{-1}$ , or about  $1.2 \text{ \AA}$  at 5000 Å, we expected to be able to make measurements of  $\alpha^2$  that were accurate to about  $1.2 \times 10^{-3}$ . As we shall see in § 6 (cf. Table 4 of § B of the Appendix), the average quoted error for an individual measurement of  $\alpha^2$  is  $1.8 \times 10^{-3}$ , somewhat larger (but not much larger) than our expected error.

### 5. Sample selection tests

We begin this section with some introductory remarks, made in § 5.1, about the sample and the sample selection. In the last four subsections of this section, §§ 5.2–5.5, we define four standard tests that were used to select the standard sample of quasar spectra from which we have determined

our best estimates of  $\alpha^2$  and  $\alpha^{-2}d\alpha^2/dt$ . Our standard sample, discussed in § 6, passes all four of the tests as described here. We present in § 7.1 a number of variations of the standard tests.

## 5.1. Introductory remarks about the spectra and the sample selection

### 5.1.1. Spectra used

We list in Table 5 of § B of the Appendix each of the 107 quasars in the SDSS EDR sample that have passed at least three of the four standard tests that we describe later in this section. Table 5 shows which of the four tests each quasar satisfies. The table also gives the measured value of  $\eta$  [see Eq. (15)] for every quasar that we have considered. If the reader would like to perform a different data analysis using our sample, this can easily be accomplished with the aid of Table 5, Eqs. (1)-(7), and Eq. (16).

Although the spectra that we use here were obtained from the SDSS Early Data Release, the spectral reductions that we use are significantly improved over the reductions given in the EDR. Improvements in the reduction code are described in Burles and Schlegel (2003).

As described in § 3, the four standard tests were developed using an initial sample of 313 quasars in the EDR data of SDSS that could potentially show both of the [O III] emission lines. The range of redshifts that was included in this initial sample is  $z = 0.163$  to  $z = 0.799$ . The complete EDR sample of quasars that we have studied includes 702 quasars with redshifts ranging from  $z = 0.150$  to  $0.799$ . A total of 24 out of 313 quasars in our initial sample passed all four of the tests described below. In our final sample, 44 quasars passed all four tests. In what follows, we shall refer to the 24 accepted quasar spectra as our “initial sub-sample” and the 44 total accepted quasars as our “standard” sample.

Unfortunately, the majority of the EDR spectra that we examined were not suitable for measurement. In nearly all of these unsuitable spectra, the O III lines did not stand out clearly above the continuum or above the noise. In a very few cases, we encountered a technical problem processing the spectra. As the first step in our ‘blind analysis’, before we imposed our four standard tests, we threw out unsuitable spectra by requiring that both of the O III lines have a positive equivalent width and that the fractional error in  $\alpha^2$ , determined from Eq. (5), be less than unity. Only 260 out of the 702 quasar spectra (37%) in which the O III lines could have been measured passed this preliminary filtering and were subjected to the standard four tests to determine the standard sample. *Post facto*, we checked that our results were essentially unchanged if we omitted this preliminary cut on unsuitable spectra, namely: the standard sample we analyze increased from 44 to 47 objects, the sample average of  $\langle \alpha(z) \rangle$  decreased by 0.002%, and the calculated error bar increased by 0.4%. We chose to impose the preliminary cut on suitable spectra because it increased our speed in analyzing a variety of alternative cuts discussed in § 7.

### 5.1.2. Standard cuts

The standard cuts described in the following subsections were imposed in the ‘blind’ phase of our analysis in order to make sure that the accepted spectra were of high quality and that the line shapes of the 5007 Å and 4959 Å lines were the same. Although we were seeking to eliminate any sources of biases by eliminating problematic spectra before we made the measurements, we have found *post facto* no evidence that omitting the any of the cuts would have led to a systematic bias.

We wanted to guard against contamination by H $\beta$  emission and to ensure that the signal to noise ratio was high. We also devised two tests that checked on the similarity of the two line shapes, the KS test discussed in § 5.2 and the line peak test described in § 5.3. In practice, all of these tests, with the exception of the check on H $\beta$  contamination, are designed to prevent noise fluctuations or unknown measuring errors from distorting the shape of one or both of the emission line profiles.

We shall see in § 7 that we could have been less stringent in imposing *a priori* criteria for acceptance of quasar spectra. We describe in § 7 the results that were obtained for four separate samples in which we omitted a different one of each of the four standard tests described in § 5.2–§ 5.5. We also present the results of analyses made using a variety of weaker versions of the four selection tests discussed in the present section. Although we obtain larger samples by using less stringent acceptance criteria, the final results for the time dependence of  $\alpha$  are robust, essentially independent of the form and number of the selection tests. Essentially, we can trade off spectral quality versus number of accepted spectra without significantly changing the final conclusion.

Figure 3 shows the spectrum of SDSS 105151-005117,  $z = 0.359$ , which easily passes all of the selection criteria described below. If all of the quasar spectra were as clean and as well measured as the spectrum of SDSS 105151-005117, no selection tests would be required. We also show in the right hand panel of Figure 3 the continuous spline fit of the shape of the 5007 Å line that, when the center is shifted in wavelength and the amplitude of the curve is decreased by a constant factor ( $A$ ), best-matches the measured data points for the 4959 Å line shape.

Figure 4 and Figure 5 illustrate the reasons why we need to impose selection criteria, or tests, to determine which quasar spectra can yield precise measurements of the wavelengths of the redshifted [O III] lines. Figure 4 shows the measured spectrum shape for four different quasars and Figure 5 shows, for the same four quasars, the best spline fits of the 5007 Å line shapes to the measured shape of the 4959 Å line. The various panels show spectra in which the measurements are compromised by different problems. In the upper left panels of Figure 4 and Figure 5, the [O III] lines have somewhat different shapes and in the upper right panels the peaks of the two lines can not be lined up precisely by a linear shift in wavelengths. In the lower left panels, the H $\beta$  line is so strong that it might distort the profile of the 4959 Å line. The spectra in the lower right panels have too low a signal to noise ratio to allow a precise measurement.

In the following subsections, we shall define more quantitatively the criteria for passing these four tests. We have formulated the tests as computer algorithms that can be applied quickly and

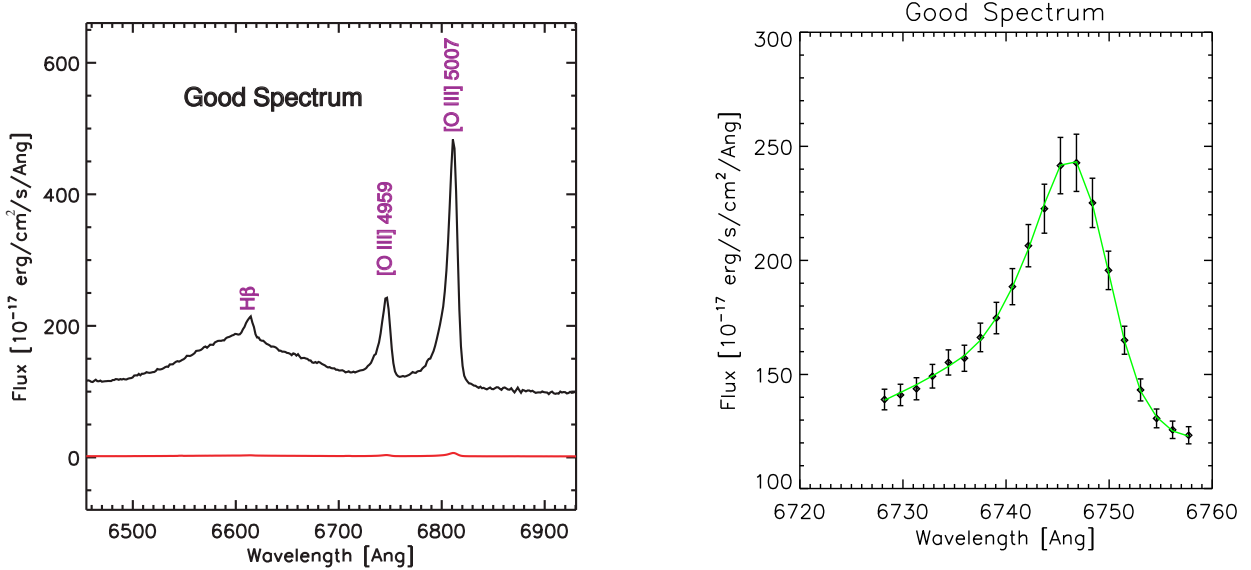


Fig. 3.— A good spectrum. The figure shows the spectrum of SDSS 105151-005117, which is also PG 1049-005. The quasar has a redshift of  $z = 0.359$ . The quasar spectrum easily passes all four of the tests described in § 5. The left panel shows the measured quasar energy spectrum in the wavelength region of interest. The approximately horizontal line near the zero flux level represents the estimated total error in the flux at each pixel. The right hand panel shows as a continuous curve the best-fit spline to the measured shape of the 5007 Å line, after shifting the line center ( $\eta$ ), decreasing the amplitude ( $A$ ), and super-imposing the spline fit on the measured data points of the 4959 Å line.

easily to numerical spectra.

We describe in § 5.2 the Kolmogorov-Smirnov test that we have applied to the emission line shapes in order to select acceptable quasar spectra. In § 5.3, we describe a test which requires that the peaks of the two emission lines essentially lie on top of each other when the line profiles are optimally shifted and rescaled. We present in § 5.4 a test that eliminates quasar spectra with a large H $\beta$  contamination of the 4959 Å line. Finally, we describe in § 5.5 a requirement that the area under the 5007 Å line be measured with a high signal-to-noise ratio. For brevity, it is convenient to refer to these tests as the KS, line peak, H $\beta$ , and signal-to-noise criteria.

## 5.2. Kolmogorov-Smirnov test

We represent the shapes of the emission line profiles by the seven measured flux values that are centered on the line peak. We then use a Kolmogorov-Smirnov (KS) test to determine whether the seven flux values centered on the peak of the 4959 Å line shape are, after multiplying by a constant factor  $A$  (see Eq. 12 and related discussion) consistent with being drawn from the same distribution as the seven flux values centered on peak of the 5007 Å line shape. The spectrum in the upper left

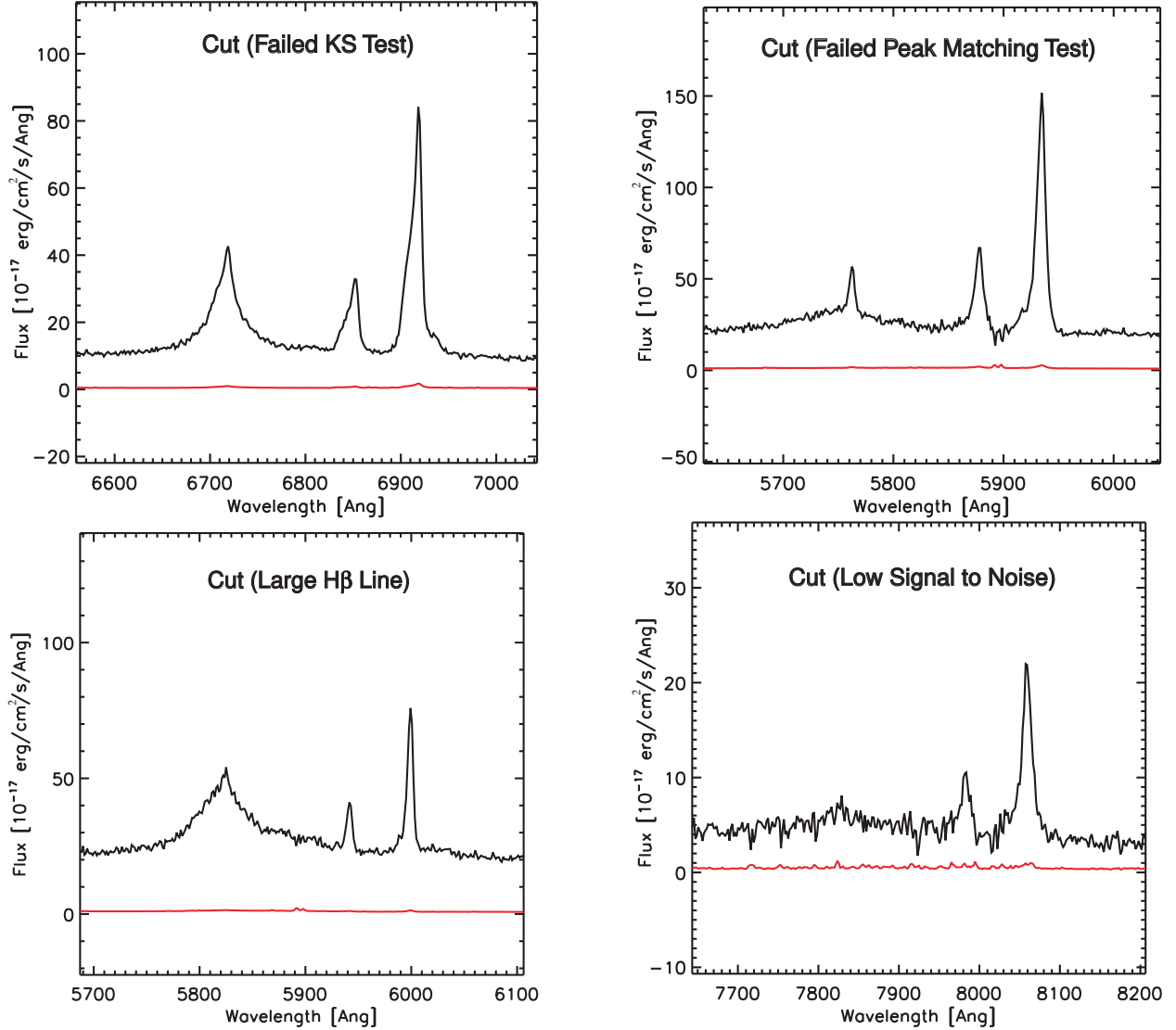


Fig. 4.— Examples of four failed spectra. The figure shows examples of spectra that failed each of the tests described in § 5. The spectrum in the upper left panel failed the KS test (cf. § 5.2); the upper right panel shows a spectrum in which the peaks failed to line up correctly (cf. § 5.3). The lower left panel displays a spectrum in which the H $\beta$  line is so large that it might contaminate the [O III] 4959 Å (cf. § 5.4); the lower right panel shows a spectrum in which the signal to noise ratio is too low to permit an accurate measurement of the splitting between the two [O III] emissions lines (cf. § 5.5).

hand panel of Figure 4 was rejected because the two [O III] lines have slightly different shapes. For an unknown reason (which could be an instrumental or measuring error or simply a fluctuation), the 4959 Å line has a slight extra contribution on the short wavelength side of the line profile.

If the two line shapes are the same before being affected by noise and measuring errors, as

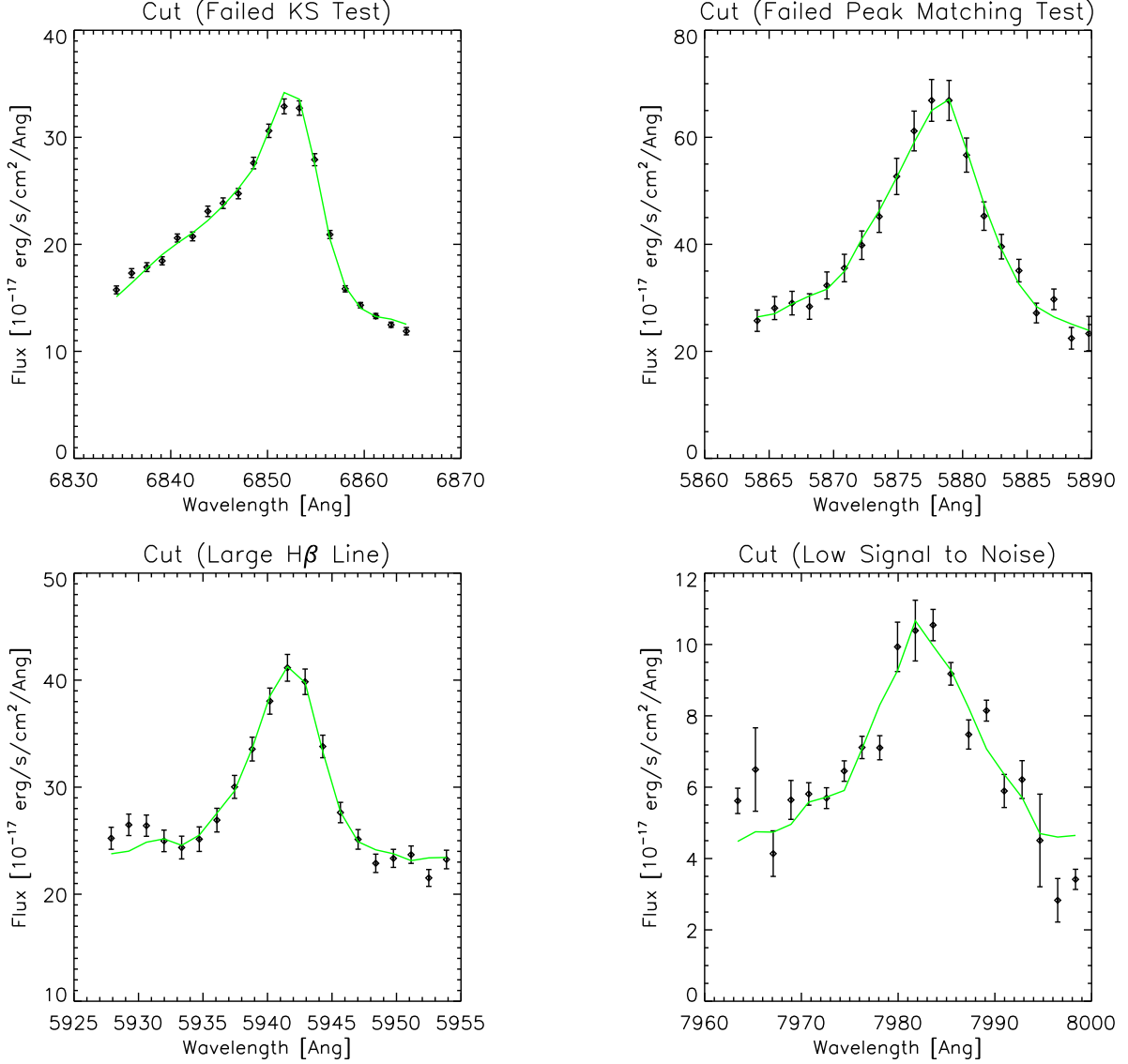


Fig. 5.— Examples of four failed fits. The quasar emission lines shown in this figure are the same as are shown in Figure 4. For each of the four examples of failed spectra shown in Figure 4, Figure 5 shows the corresponding best (but failed) spline fit of the measured shape of the 5007 Å line (continuous curve) to the measured shape (points with error bars) of the 4959 Å line.

required by the analysis described in § 4, then the two lines will generally pass a KS test. We set our level for acceptance such that there are only a few false negatives, i.e., spectra incorrectly rejected. In principle, there could be some false positives since the KS test does not require that the flux values match in wavelength as well as in intensity. In practice, false positives of this kind essentially never occur.

We require that the two sets of 7 flux values be drawn from the same distribution to a confidence level (C.L.) corresponding to  $2\sigma$  (95% C.L.). From our initial sample of 313 quasars in the redshift range that allowed the observation of the [O III] lines, 13 quasars failed this test but no other test. Five of the 13 quasars that failed the test had values of  $\alpha^2$  that differed by at least  $2\sigma$  from the sample average of  $\alpha^2$ . In the full EDR sample, 29 quasars failed only this test. Out of the 260 quasars that passed the preliminary spectral quality test described in § 5.1, only 80 passed the KS test. Out of the total sample of 702 objects with redshifts that permitted the measurement of the O III lines, only 108 passed the KS test.

The requirement that the shapes of the 5007 Å and 4959 Å lines be similar according to the KS test is our most stringent test.

We show in § 7 that the results are essentially unchanged if we use the central 11 flux values instead of the central 7 values (see row four of Table 1 and Table 2) or if we omit the KS test entirely (see row eight of Table 1 and Table 2).

### 5.3. Lining up the peaks

We require that the peak of the 4959 Å line and the peak of the shifted 5007 Å line lie in the same pixel, for the best-fit value of  $\eta$ . The demand that the two peaks be lined up after the 4959 Å line is optimally shifted strengthens the constraint that the two shapes be the same. Since this test requires that the peaks line up but does not constrain the shift  $\eta$ , the test enforces the requirement that the shapes of the two lines be the same but does not constrain the possible values of  $\alpha$ . In principle, this test may occasionally reject otherwise acceptable spectra if the peak of one of the lines lies very near the boundary between two pixels. In the initial sample, only two quasars failed this test but no other test. Both of the quasars which failed were  $2\sigma$  outliers. In the full EDR sample, nine quasars failed only this test. Out of the 260 quasars that passed the preliminary spectral quality test described in § 5.1, 138 passed the test of the lining up of the peaks. From the total sample of 702 objects with appropriate redshifts for measuring O III lines, 254 passed the line peak test.

If we omit the line peak test, the sample size increases by nine objects, but the overall results are unchanged (see row nine of Table 1 and Table 2).

### 5.4. H $\beta$ contamination

The H $\beta$  line, which is centered at 4861 Å, can contaminate the 4959 Å line if H $\beta$  is too strong. Moreover, the presence of a strong H $\beta$  line could in principle distort the continuum fit. Therefore, we require that the area under the H $\beta$  line be no more than twice the area under the 5007 Å line. In practice, this requirement ensures that the contamination of the 4959 Å line from the H $\beta$  line

is less than the contamination from the 5007 Å line. In our initial sample, three quasars failed only this test. In the full EDR sample, four quasars failed only this test. None of the quasars that failed this test were  $2\sigma$  outliers. Out of the 260 (702) quasars that passed the preliminary spectral quality test (for which the quasar redshift permitted the measurement of the O III lines), 207 (333) passed the H $\beta$  test.

The results of the analysis are essentially unchanged if the H $\beta$  test is omitted entirely (see row ten of Table 1 and Table 2).

### 5.5. Signal-to-Noise Test

Our final test is designed to eliminate spectra that are too noisy to make an accurate measurement of  $\alpha^2$ . We require that the area under the 5007 Å line be measured to an accuracy of  $\pm 5\%$  as determined using the errors estimated from the Spectro 2-D code (Burles and Schlegel 2003). In other words, we require that the signal-to-noise ratio for the line intensity is at least 20:1. Six quasars failed only this test in our initial sample; one of the failed quasars was a  $2\sigma$  outlier. In the full EDR sample, 7 quasars failed only this test. Out of the 260 (702) quasars that passed the preliminary spectral quality test (for which the O III lines could have been measured), 105 (404) passed the signal-to-noise test.

The results are essentially unchanged if the signal-to-noise test is omitted entirely (see row eleven of Table 1 and Table 2).

## 6. Standard Sample

In this section, we discuss the results of our analysis of the spectra of the 44 objects in our Standard Sample. For the reader's convenience, we give in Table 4 of § B of the Appendix the values of the redshift, the measured quantity  $\eta(z)$  [defined by Eq. (15)] that determines  $\alpha^2(z)$ , and the relative scaling factor,  $A$  (defined in § 4), for all the QSO's in the Standard Sample.

Figure 6 shows, for the 44 standard QSO's, how the measured values of  $\alpha$  depend upon cosmic lookback time. It is apparent from a chi-by-eye fit to Figure 6 that there is no significant time dependence for the measured values of  $\alpha$  in our Standard Sample. The lookback time shown in Figure 6 is  $H_0 t$ , which is independent of the numerical value of  $H_0$  (see Eq. 8).

We present in § 6.1 the average value of  $\alpha$  measured for our Standard Sample, as well as the best-fit slope,  $\langle d\alpha(t)/dt \rangle$ . In § 6.2, we describe how we have calculated the bootstrap errors for the sample properties.

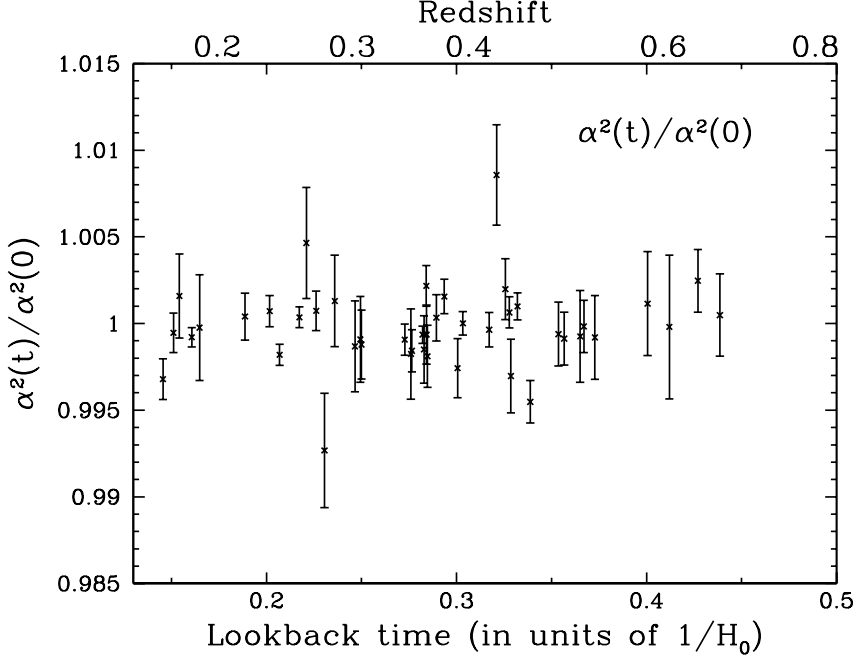


Fig. 6.— The fine-structure constant versus cosmic time. For our standard sample of 44 quasar spectra, the figure shows the measured values of  $\alpha(t)$  versus cosmic lookback time. The measurements are consistent with a value of  $\alpha$  that does not change with cosmic time. The lookback time is expressed in units of  $H_0^{-1} = 1.4 \times 10^{10} \text{ yr}^{-1}$  [see Eq. (8)].

### 6.1. Average and Slope for the Standard Sample

The first row of Table 1 shows that the weighted average value of  $\alpha^2(z)$  for our standard sample is

$$\frac{\langle \alpha^2(z) \rangle}{\alpha^2(0)} = 0.9996 \pm 0.0002, \quad (17)$$

where we have calculated each  $\alpha^2(t)/\alpha^2(0)$  from Eq. (5). We have used the local value of  $\alpha^2(0)$  (or, more precisely,  $R(0)$ , see Eq. 4) in Table 1 and in Eq. (17) only to establish the scale. We have not made use of the local measurement of  $R(0)$  in either Table 1 or Eq. (17).

It is conventional to represent cosmological variations of  $\alpha$  in terms of the average fractional change over the time probed by the sample. In this language, the limit given in Eq. (17) is

$$\frac{\Delta \alpha}{\alpha(0)} = (-2 \pm 1.2) \times 10^{-4}. \quad (18)$$

Table 1: Average value of alpha. The table presents in column three the measured weighted average value of  $\alpha^2/\alpha^2(0)$  for our standard sample as well as the measured average for 17 alternative cuts, defined in § 7.1, on the data. The number of quasar spectra that pass the cuts defining each sample is given in the second column. No alternative sample produces an average value of  $\alpha$  significantly different from the value obtained for the standard sample.

Sample	Sample Size	Average $\alpha^2/\alpha^2(0)$
Standard sample	44	$0.9996 \pm 0.0002$
Unweighted errors	44	$0.9997 \pm 0.0004$
Strict $H\beta$ limit	29	$0.9992 \pm 0.0003$
Signal-to-noise of 10:1	50	$0.9996 \pm 0.0002$
11 point KS test	70	$0.9997 \pm 0.0002$
EW not area	44	$0.9996 \pm 0.0002$
$\chi^2$ instead of KS	58	$0.9996 \pm 0.0002$
Omit KS test	73	$0.9996 \pm 0.0002$
Omit peak line up	53	$0.9996 \pm 0.0002$
Omit $H\beta$ test	48	$0.9996 \pm 0.0002$
Omit signal-to-noise test	51	$0.9996 \pm 0.0002$
Remove worst outlier	43	$0.9995 \pm 0.0002$
$z < 0.3622$	22	$0.9994 \pm 0.0003$
$z > 0.3622$	22	$0.9999 \pm 0.0004$
$\Omega_m = 1, \Omega_\Lambda = 0$	44	$0.9996 \pm 0.0002$
$\Omega_m = 0, \Omega_\Lambda = 1$	44	$0.9996 \pm 0.0002$
Add $R(0)$ and $\sigma_0$	45	$0.9998 \pm 0.0002$
Add $R(0)$ and $0.1\sigma_0$	45	$0.9998 \pm 0.0002$

The average lookback time for our Standard Sample is

$$\langle t \rangle = \frac{0.28}{H_0} = 3.8 \times 10^9 \text{ yr}^{-1} \left( \frac{72 \text{ km s}^{-1} \text{Mpc}^{-1}}{H_0} \right). \quad (19)$$

Therefore, the characteristic variation of  $\alpha$  permitted by our Standard Sample is

$$\frac{\Delta \alpha}{\langle t \rangle \alpha} = (-5 \pm 3) \times 10^{-14} \text{ yr}^{-1}. \quad (20)$$

The mean (median) redshift for the Standard Sample is  $z = 0.37$  ( $z = 0.36$ ).

The best-fit value of  $d\alpha/\alpha dt$  can be obtained by fitting the observed values of  $\alpha^2(t)$  given in Table 4 of § B of the Appendix to a linear relation, Eq. (6), with a slope defined by Eq. (7). Using the slope given in Table 2, we find for our Standard Sample

$$\frac{1}{\alpha} \frac{d\alpha}{dt} = \frac{H_0 \times \text{Slope}}{2} = (9.6 \pm 7.4) \times 10^{-14} \text{ yr}^{-1} \left( \frac{H_0}{72 \text{ km s}^{-1} \text{Mpc}^{-1}} \right). \quad (21)$$

Table 2: Best linear fit. Here  $\alpha^2(t) = \alpha_{\text{fit},0}^2[1 + H_0 St]$ , where the slope  $S$  is defined by Eq. (7). The value of the intercept,  $\alpha_{\text{fit},0}^2$  and the slope  $S$  are both calculated from the quasar measurements summarized in Table 5. In the table, the value of  $\alpha_{\text{fit},0}^2/\alpha^2(\text{local meas.})$  is defined by Eq. (5). Except where explicitly stated otherwise, the time  $t$  is calculated from Eq. (8) for a universe with the present composition of  $\Omega_m = 0.3, \Omega_\Lambda = 0.7$ .

Sample	Sample Size	$\alpha_{\text{fit},0}^2/\alpha^2(\text{local meas.})$	Slope $S$
Standard sample	44	$0.9987 \pm 0.0007$	$0.0026 \pm 0.0020$
Unweighted errors	44	$0.9988 \pm 0.0009$	$0.0022 \pm 0.0020$
Strict H $\beta$ limit	29	$0.9975 \pm 0.0009$	$0.0048 \pm 0.0024$
Signal-to-noise of 10:1	50	$0.9988 \pm 0.0007$	$0.0024 \pm 0.0020$
11 point KS test	70	$0.9989 \pm 0.0007$	$0.0022 \pm 0.0018$
EW not area	44	$0.9987 \pm 0.0007$	$0.0026 \pm 0.0020$
$\chi^2$ instead of KS	58	$0.9987 \pm 0.0007$	$0.0024 \pm 0.0020$
Omit KS test	73	$0.9989 \pm 0.0007$	$0.0021 \pm 0.0018$
Omit peak line up	53	$0.9988 \pm 0.0007$	$0.0019 \pm 0.0020$
Omit H $\beta$ test	48	$0.9986 \pm 0.0007$	$0.0028 \pm 0.0019$
Omit signal-to-noise test	51	$0.9988 \pm 0.0007$	$0.0024 \pm 0.0020$
Remove worst outlier	43	$0.9987 \pm 0.0007$	$0.0023 \pm 0.0020$
$z < 0.3622$	22	$0.9988 \pm 0.0012$	$0.0023 \pm 0.0042$
$z > 0.3622$	22	$0.9994 \pm 0.0019$	$0.0010 \pm 0.0041$
$\Omega_m = 1, \Omega_\Lambda = 0$	44	$0.9989 \pm 0.0006$	$0.0015 \pm 0.0012$
$\Omega_m = 0, \Omega_\Lambda = 1$	44	$0.9985 \pm 0.0009$	$0.0037 \pm 0.0029$
Add $R(0)$ and $\sigma_0$	45	$0.9993 \pm 0.0009$	$0.0010 \pm 0.0034$
Add $R(0)$ and $0.1\sigma_0$	45	$0.9993 \pm 0.0009$	$0.0010 \pm 0.0034$

The slope given in Eq. (21) is obtained using only measurements made on the spectra of the 44 quasars in our standard sample. No independent knowledge of  $\alpha(0)$  is used. Hence, the limit implied by Eq. (21) is self-calibrating.

In the first rows of Table 1 and Table 2, we give the best-fit parameters, as well as their uncertainties, that were computed using the bootstrap errors (see discussion of bootstrap errors in § 6.2 below). In the second rows of Table 1 and Table 2, we give the same quantities but this time computed by assuming that all the errors are the same and equal to the average of the formal measuring errors used for the first row calculations. The results are essentially the same.

## 6.2. Bootstrap estimate of uncertainties

The errors quoted in this section and elsewhere in the paper represent  $1\sigma$  uncertainties calculated using a bootstrap technique with replacement. For readers interested in the details, this is

exactly what we did to find the uncertainties in the quantities calculated for the standard sample. We created  $10^5$  simulated samples by drawing 44 objects at random and with replacement from the real sample. For each of these simulated realizations, we calculate a weighted average of the sample. We then determine the average and the standard deviation from the distribution, which was very well fit by a Gaussian, of the weighted averages of the  $10^5$  simulated samples.

We demonstrate in § 7 (cf. rows 1 and 2 of Table 1 and Table 2) that the sample averages for the time-dependence of  $\alpha$  are rather insensitive to the estimated sizes of the individual error bars. By construction, the inferred uncertainties only depend on the relative sizes of the assigned error bars in the observed sample. The estimated errors in the standard sample could all be multiplied by an arbitrary scale factor without affecting the final inferred uncertainty for the sample average. Even the relative errors are not very important in the present case, because all the errors are rather similar in the standard sample.

## 7. Results for 18 Different Samples

Table 1 and Table 2 present the results obtained for 17 samples of quasar spectra in addition to our Standard Sample. These additional samples were defined by modifying in various ways the selection criteria, described in § 5, that were used to select the Standard Sample. The last one of the 17 alternate samples shown in Table 1 and Table 2 contains a hypothetical data point; this sample includes a local measurement of  $\alpha^2$  that is ten times more accurate than the best currently-available local measurement.

The 16 additional data samples in rows 2–17 of Table 1 and Table 2 were created from the SDSS data sample using less restrictive selection criteria. The sample presented in row 18 was created in order to determine whether a much improved measurement of  $R(0)$  would significantly affect the precision with which the time-dependence of  $\alpha$  can be investigated using O III measurements.

These additional data samples were created in order to test the robustness of our conclusions regarding the lack of time dependence of  $\alpha$ , conclusions that are stated in § 6, especially Eq. (18) and Eq. (21). We answer here the following question: Does the lack of measured time dependence for  $\alpha$  depend upon how we define the data sample? The answer is no. Our conclusions regarding the time dependence of  $\alpha$  are robust; the conclusions are the same for all the variations we have made on the selection criteria that define the samples.

We begin in § 7.1 by describing the 17 samples that we have studied in addition to the Standard Sample. We discuss in § 7.2 the numerical results obtained for the alternative samples.

### 7.1. Definitions of Alternative Samples

In this section, we describe briefly how the 17 non-standard data samples were determined. In the comments below, we only state how the defining criteria are changed for the alternative samples. For each alternative sample, each test discussed in § 5 that is not mentioned explicitly below has been used in selecting the alternative sample. The descriptions are ordered in the same way as the samples appear in Table 1 and Table 2.

**Unweighted errors.** This sample is created from the data of the Standard Sample by artificially setting all of the errors to be equal.

**Strict H $\beta$  limit.** The H $\beta$  limit used in defining this sample is twice as strict as for the Standard Sample. The area under the H $\beta$  emission line is required to be less than or equal to the area under the [O III] 5007 Å line. This stronger requirement removes 15 of the 44 quasars in the standard sample.

**Signal-to-noise of 10:1.** For our standard sample we require that the area under the 5007 Å emission be measured to an accuracy of 5%, corresponding to a signal-to-noise ratio of 20:1. We relax this signal-to-noise criterion to 10:1 for this alternative, which increases the standard sample by an additional 6 quasars.

**11 point KS test.** Eleven points centered on the peaks of the [O III] 4959 Å line and the 4007 Å line are used in carrying out the KS test, instead of the 7 points used in defining the standard sample. This change in the number of points used increases the sample size by more than 50%, from 44 to 70 quasars.

**Equivalent widths rather than areas.** It is common in astronomy to describe emission lines in terms of equivalent width, the number of Angstroms of continuum flux that is equal to the total flux in an emission line. We have required for this alternative sample that the uncertainty in the measured equivalent width of the 5007 Å line be no more than 5%, i.e., that the signal to noise ratio of the measured equivalent width be 20:1. For the Standard Sample, the 20:1 requirement is made on the area under the emission line, not on the equivalent width. Replacing the requirement on the accuracy of the measurement of the area under the 5007 Å emission line by a requirement on the equivalent width has no effect on the allowed sample. We note that the average (median) equivalent width of the 5007 Å line in the Standard Sample is 68 Å (57 Å).

**$\chi^2$  instead of KS.** For this sample, we replaced the KS test with a  $\chi^2$  test. We used the 20 pixel region of the spectrum centered on the expected position of the 4959 Å line and compared the shape of this line with the best-fit shifted and rescaled shape of the 5007 Å line. We require that  $\chi^2$  per degree of freedom be less than one. We obtain a total sample size of 58 if we use the  $\chi^2$  test instead of the KS test.

**Omit KS test.** We now describe the results of eliminating, one at a time, each one of our criteria for inclusion in the standard sample. Our most stringent test is the KS test. If we omit this test entirely, the alternative sample is increased by 29 objects to a total sample of 73 quasars. This is the largest sample we consider.

**Omit peak line up.** The requirement that the peaks of the 5007 Å and 4959 Å lines line up within one pixel may occasionally eliminate some good spectra. We have omitted the lining-up requirement, which increases the standard sample by an additional 9 quasars.

**Omit  $H\beta$  test.** For the standard sample, we have placed a stringent requirement on the possible  $H\beta$  contamination. If we omit the  $H\beta$  test entirely, the sample is increased by 4 quasars.

**Omit signal-to-noise test.** We omit entirely the signal-to-noise test, increasing the sample by 7 additional objects.

**Remove worst outlier.** We remove from the standard sample the quasar that has a value of  $\alpha^2$  that differs the most from the average value of  $\alpha^2$  within the standard sample. This object is  $3.4\sigma$  from the standard sample average.

**Require  $z < 0.3622$ .** We split the standard sample into two equal parts in order to test whether  $\alpha^2$  is the same in the low and the high redshift halves of the sample. This sample is the low Z half of the standard sample.

**Require  $z > 0.3622$ .** This is the high redshift half of the standard sample.

$\Omega_m = 1.0$ ,  $\Omega_\Lambda = 0.0$ . To test for the sensitivity of our results to our assumptions regarding cosmological parameters, we recalculated all quantities using cosmological times appropriate for an extreme universe with  $\Omega_m = 1.0$ ,  $\Omega_\Lambda = 0.0$ .

$\Omega_m = 0.0$ ,  $\Omega_\Lambda = 1.0$ . We also analyzed the data using the extreme cosmological parameters  $\Omega_m = 0.0$ ,  $\Omega_\Lambda = 1.0$ .

**Add  $R(0)$  and  $\sigma(0)$ .** We added to the standard sample the local measurement summarized in Eq. (2)-Eq. (4).

**Add  $R(0)$  and  $0.1\sigma(0)$ .** This sample is hypothetical. We supposed that the accuracy of the local measurement could be improved by a factor of 10. The purpose of studying this sample was to investigate whether a better local measurement would improve the over-all accuracy of the determination of the time dependence of  $\alpha$ .

We have not considered samples in which a precise external value of  $\alpha$  is introduced, a value of  $\alpha$  determined by measurements that do not involve the O III emission lines. In order to use external values of  $\alpha$ , we would need to rely upon an extremely accurate theoretical calculation of the fine structure splitting for the two O III lines. This reliance would depart from the empirical

approach we have adopted; it would subject our analysis to some of the same concerns that we express in § 8 with respect to the Many-Multiplet method. We limit ourselves to considering ratios of O III wavelengths [see Eq. (1) and Eq. (5)], since many recognized systematic uncertainties (and perhaps also some unrecognized uncertainties) are avoided in this way.

## 7.2. Numerical results for Alternate samples

We discuss in this subsection the numerical results for the 17 alternative samples including their average values (§ 7.2.1), their slopes (§ 7.2.2), the influence of  $R(0)$  (§ 7.2.3), and the insensitivity of the sample errors to the estimates of the errors for individual measurements of  $\alpha^2$  (§ 7.2.4).

### 7.2.1. Average values

Table 1 shows that all of the samples we have considered yield average values for  $\alpha^2$  that lie within the range

$$\frac{\langle \alpha^2 \rangle}{\alpha^2(0)} = 0.9996^{+0.0002}_{-0.0004}, \quad (22)$$

where the fiducial value of  $\langle \alpha^2 \rangle / \alpha^2(0) = 0.9996$  was chosen because it is the average value for the standard sample. Since the calculated errors on the average of each sample are between  $\pm 0.0002$  and  $\pm 0.0004$ , it is clear from Eq. (22) that all of the samples shown in Table 1 give consistent values for  $\langle \alpha^2 \rangle / \alpha^2(0)$ .

The results given in Table 1 are all consistent with a fine-structure constant that does not vary with time. The characteristic variation permitted is  $\Delta \alpha / \langle t \rangle \alpha = (-5 \pm 3) \times 10^{-14} \text{ yr}^{-1}$  [see Eq. (20)].

### 7.2.2. Slopes

Table 2 gives the best-fitting slopes,  $S$ , for an assumed linear dependence of  $\alpha^2(t)$  on  $t$ . All of the slopes are consistent with zero within  $2\sigma$ . There is no significant evidence for a time dependence of  $\alpha$  in any of the samples we have considered. Using the quoted value of  $H_0$  to convert the slopes,  $S$ , given in Table 2 to time derivatives (and including the factor of two that relates the slopes of  $\alpha^2(t)$  and  $\alpha(t)$ ), we conclude that [cf. Eq. (21)]

$$\left| \frac{1}{\alpha} \frac{d\alpha}{dt} \right| < 10^{-13} \text{ yr}^{-1}. \quad (23)$$

### 7.2.3. The role of the local value of $R(0)$

The various samples for which results are given in the first 16 rows of Table 1 and Table 2 do not include any local measurements of  $R$  [cf. Eq. (1)]. The last two rows of Table 1 and Table 2 contain an additional data point representing the local value of  $R(0)$ , as presented in Eq. (4).

We see from rows 17 and 18 of Table 1 and Table 2 that adding the local value of  $R(0)$  does not change significantly either the sample average of  $R(0)$  or the slope describing the time dependence. Even if one assumes, as was done in constructing row 18 of Table 1 and Table 2, that the uncertainty in the local value of  $R(0)$  could be reduced by a factor of ten, there would still not be a significant impact on the accuracy with which the time dependence of  $\alpha^2$  would be known. The existing error on  $R(0)$  is already much less than the other errors that enter our analysis.

### 7.2.4. Errors

The bootstrap method that we have used to calculate the errors is insensitive to the average size of the errors made in individual measurements of  $\alpha^2$  and depends only weakly on the relative errors (see the discussion of bootstrap errors in § 6). The robustness of the bootstrap errors can be seen most clearly by comparing the results for rows one and two in Table 1 and Table 2. In row one, the bootstrap uncertainty was estimated for the standard sample making use, in computing an average for each of the  $10^5$  simulated samples, of the actual errors determined from our individual measurements. In row two, the bootstrap uncertainty was estimated by assuming that the errors on all measurements were identical. The results shown in rows one and two of Table 1 and Table 2 are essentially identical for both the sample average and the time dependence of  $\alpha$ .

## 8. Comparison of O III method with Many-Multiplet method

In this section, we compare the O III emission line method for studying the time-dependence of the fine-structure constant with what has been called the ‘Many-Multiplet’ method. The Many-Multiplet method is an extension of, or a variant on, previous absorption line studies of the time-dependence of  $\alpha$ . We single out the Many-Multiplet method for special discussion since among all the studies done so far on the time dependence of the fine-structure constant, only the results obtained with the Many-Multiplet method yield statistically significant evidence for a time dependence. All of the other studies, including precision terrestrial laboratory measurements (see references in Uzan 2002) and previous investigations using quasar absorption lines (cf. Bahcall, Sargent, & Schmidt 1967; Wolfe, Brown, & Roberts 1976; Levshakov 1994; Potekhin & Varshalovich 1994, Cowie & Songaila 1995; and Ivanchik, Potekhin, & Varshalovich 1999) or AGN emission lines (Savedoff 1956; Bahcall & Schmidt 1967), are consistent with a value of  $\alpha$  that is independent of cosmic time. The upper limits that have been obtained in the most precise of these previous

absorption line studies are  $|\Delta\alpha/\alpha(0)| < 2 \times 10^{-4}$ . None of the previous absorption line studies has the sensitivity that has been claimed for the Many-Multiplet method.

We first describe in § 8.1 the salient features of the Many-Multiplet method. Then in § 8.2 we compare and contrast the Many-Multiplet method for measuring the time-dependence of  $\alpha$  with the O III method.

### 8.1. The Many-Multiplet method

In the last several years, a number of papers have discussed the “Many-Multiplet” method for determining the time dependence of  $\alpha$  using quasar absorption line spectra (see Dzuba, Flambaum, & Webb 1999a,b; Webb et al. 1999; Murphy et al. 2001a,b; and Webb et al. 2002, as well as references quoted therein). Because of the many different atomic transitions that are used and because of the measurement of absolute wavelengths, the method has a potential sensitivity that is much greater than the sensitivity that has been achieved with the O III or any other astronomical method. The Many-Multiplet collaboration has inferred a change in alpha with cosmic epoch,  $\Delta\alpha/\alpha(0) = (-0.7 \pm 0.2) \times 10^{-5}$ , over a redshift range from  $z = 0.2$  to  $3.5$  (see especially Murphy et al. 2001a,b and Webb et al. 2002 and references to earlier in this paragraph).

The Many-Multiplet method compares the measured wavelengths of absorption (not emission) lines seen in quasar spectra with the measured or computed laboratory wavelengths of the same lines. Lines from the ions Mg I, Mg II, Al II, Si II, Cr II, Fe II, Ni II, and Zn II are used (cf. Table 1 of Murphy et al. 2001b). In addition, different multiplets from the same ion are used. The lower redshift (smaller lookback time) results are based upon measurements made using Mg I, Mg II, and Fe II, while the larger redshift results use lines observed from Al II, Al III, Si II, Cr II, Ni II, and Zn II.

In order to increase the measuring precision, the Many-Multiplet (see Murphy et al. 2001b) “...is based on measuring the wavelength separation between the resonance transitions of *different ionic species* with no restriction on the multiplet to which the transitions belong.” To take advantage of the relatively large values of the relativistic corrections (proportional to  $\alpha^4$ , non-relativistic energies are proportional to  $\alpha^2$ ) in the ground state atomic energies, the Many-Multiplet method uses the absolute values of the wavelengths.

As emphasized by Murphy et al. 2001b, the absolute values of the wavelengths of many individual transitions must be precisely known from laboratory experiments and measured precisely in the quasar spectra in order to reach a higher precision than is possible by measuring the ratios of fine-structure splittings to average wavelengths. In the O III method, and in the many applications of doublet splittings of absorption lines that originate on a single ground state, the relativistic terms appear only in the relatively small fine-structure splittings of the excited states of the atoms. The Many-Multiplet method utilizes the fact that atomic ground states have larger relativistic, i.e.,  $\alpha^4$ , contributions to their energies than do excited states. Instead of concentrating on splittings, in

which the ground state contributions cancel out, the Many-Multiplet method requires and makes use of the measurement of absolute wavelengths.

Sophisticated theoretical atomic physics calculations are required in order to determine how changing the value of  $\alpha$  affects the wavelengths of the different transitions employed in the Many-Multiplet method. In particular, one must calculate precisely the derivatives of the transition wavelengths with respect to  $\alpha^2$ . Therefore, Dzuba, Flambaum, & Webb (1999a,b) have developed new theoretical tools to calculate the relativistic shift for each transition of interest. They use a relativistic Hartree-Fock method to construct a basis set of one-electron orbitals and a configuration interaction method to obtain the many-electron wave function of valence electrons. Correlations between core and valence electrons are included by means of many-body perturbation theory.

How accurately must the absolute wavelengths be measured in the Many-Multiplet method? This question has not been answered directly, to the best of our knowledge, in the published papers. However, one can easily make a rough estimate of the required accuracy using the data given in Table 1 and Eqs. (4) and (5) of Murphy et al. (2001b). Using the quoted uncertainty,  $\pm 2 \times 10^{-6}$  (see Webb et al. 2001b), in a sample average value of  $[\alpha(z)/\alpha(0) - 1.0]$ , we find that wavelength measurements must be accurate to  $\sim 0.01 \text{ \AA}$  ( $q_1/\omega_0$ ) (using the notation of Webb et al. 2001b). Here  $2q_1$  is approximately equal to the partial derivative of the wavenumber,  $\omega_z$ , measured at redshift  $z$  with respect to  $\alpha(z)/\alpha(0)$ , i.e.,  $2q_1 = \partial\omega_z/\partial x$  with  $x = \alpha(z)/\alpha(0)$ . There are 23 separate transitions that are listed in Table 1 of Webb et al. (2001b) and which have been used in the Many-Multiplet measurements. For these 23 transitions, the mean and the average value of  $(q_1/\omega_0) = 0.02$ . Thus a sample average wavelength accuracy of about  $2 \times 10^{-4} \text{ \AA}$  is required to reach the quoted precision in  $\alpha(z)/\alpha(0)$ . Because the analysis of the Many-Multiplet measurements is made using all of the data together in a maximum likelihood analysis, it is not clear from the published papers how many individual lines with what individual values of  $(q_1/\omega_0)$  are used and with what weightings. Lines of such abundant elements as Mg I, Mg II, Al II, and Al III have relatively small values of  $(q_1/\omega_0)$  and therefore constrain  $\alpha(z)/\alpha(0)$  less strongly. The largest quoted values for  $(q_1/\omega_0)$  in Table 1 of Webb et al. (2001b) are for the less abundant ions of Ni II and Zn II.

The known systematic uncertainties have been discussed extensively in a series of papers by the originators of the Many-Multiplet method. These comprehensive and impressive studies cover many different topics. It is far beyond the scope of this article to discuss in detail the systematic uncertainties and the accuracy obtainable with the Many-Multiplet method. The reader is referred to an excellent presentation of the Many-Multiplet method in a series of published papers (see especially Murphy et al. 2001a; as well as Dzuba, Flambaum, & Webb 1999a,b; Webb et al. 1999; Murphy et al. 2001b; Webb et al. 2002; and the recent preprint by Webb, Murphy, Flambaum, and Curran 2002).

## 8.2. Contrasts between the O III method and the Many-Multiplet method

In this subsection, we compare briefly some practical consequences of two strategies for measuring the time dependence of  $\alpha$ , the O III method and the Many-Multiplet method. In the papers by the Many-Multiplet collaboration, there are extensive discussions of the advantages of that method so we will not repeat their arguments here. The reader is referred to the original papers of the Many-Multiplet group for an eloquent description of the virtues of their method (Dzuba, Flambaum, & Webb 1999a,b; Webb et al. 1999; Murphy et al. 2001a,b; and Webb et al. 2002).

Table 3 shows a schematic outline of the differences between the two methods.

### 8.2.1. *Ions, transitions, multiplets*

For the O III method, only one ion with one pair of transitions from the same multiplet is used.

For the Many-Multiplet method, one uses many lines from many multiplets arising from ions with different charge and mass. At the large redshifts at which the Many-Multiplet collaboration has found a time dependence for the fine-structure constant, the Many-Multiplet sample contains about 2 times as many lines in about 0.5 as many quasar spectra as we include in our standard sample (cf. Table 1 of Murphy et al. 2001a with Table 4 of this paper). The quoted error of the Many-Multiplet collaboration is typically two orders of magnitude smaller than our quoted error.

### 8.2.2. *Theory*

For the O III method, no theoretical calculations are required to determine the dependence of  $\alpha$  upon the measured quantity. As explained in § 2, the time dependence of  $\alpha^2(t)$  can be determined by measuring the ratio of the difference of two wavelengths divided by their sum [see Eq. (5)].

The situation is different for the Many-Multiplet method. Sophisticated many-body relativistic calculations (Dzuba, Flambaum, & Webb 1999a,b), including electronic correlations, are required in order to determine the way the measured wavelengths depend upon  $\alpha$  for the many different lines used in the Many-Multiplet method.

### 8.2.3. *Wavelength Measurements*

The O III method only makes use of the difference and the ratio of wavelengths, while the Many-Multiplet method requires knowing accurately the absolute values of the wavelengths for all the transitions that are used. Some systematic uncertainties that are important if one uses the absolute values of the wavelengths (needed for the Many-Multiplet method) cancel out when one considers only ratios of wavelengths (as appropriate for the O III method).

Table 3: Comparison of the O III and Many-Multiplet Methods.

	O III	Many-Multiplet
Number of ions	one	many; different $Z, A$
Transitions	one	many
Multiplets	one	many
Theory	none	relativistic, many body
Wavelengths	relative	absolute
Sample precision	0.01 Å	0.0002 Å
Velocity profiles	identical	modeled; all ions same
Line strengths	strong	weak and strong
Misidentification (or blending)	no	a concern
Full disclosure	yes	extremely difficult
Local value of $\alpha$	independent of	depends upon

For the O III method, we have achieved a sample average accuracy for the wavelength splitting of 0.01 Å, corresponding to an accuracy of individual measurements of about 0.07 Å. This accuracy corresponds to individual measurement errors of slightly better than a tenth of a pixel, which is a relatively modest precision for the high signal-to-noise spectra we have used.

The Many-Multiplet method requires a much higher measurement precision, which is characteristically of order 0.0002 Å for a sample of absorption lines with a characteristic (or mean) value of  $q_1/\omega_0$  (see § 8.1 and Webb et al. 2001b). It is not clear exactly how many lines with large values of  $q_1/\omega_0$  contribute to the sample average. One may guess crudely that the sample average might achieve an accuracy of a factor of several up to an order of magnitude better than the individual measurements. This would suggest that the required precision for individual absorption lines is of order 0.001 Å, which is very demanding, especially since the typical pixel size for the Many-Multiplet spectra is  $\gtrsim 0.03$  Å. A more precise estimate of the required accuracy can only be made by the Many-Multiplet collaboration itself using all of the detailed inputs to their overall error estimates.

#### 8.2.4. Line profiles

The emission line profile is identical for all transitions used in the O III method. Indeed, this is one of the four principal criteria employed to select the O III sample (see § 5.2). Understanding the velocity profiles of all the lines that contribute to the absorption spectra is a critical requirement for the Many-Multiplet method. Moreover, the Many-Multiplet technique requires that, for each absorption line redshift, the likelihood function be maximized with respect to a set of velocity profiles that represent the different individual cloud velocities that contribute to each of the absorption

lines. The number of velocity components and their relative velocities are not known a priori and must be solved for in the maximization process. Typically, five or more independent cloud velocities are required to fit the data. In their first paper suggesting a time-dependent fine-structure constant, the Many-Multiplet collaboration noted conservatively that an anomaly in their data might be explained by "... additional undiscovered velocity components in the absorbing gas" Webb et al. 1999).

Murphy et al. (2001b) have stressed that for the Many-Multiplet method "The central assumption in the analysis is that the velocity structure seen in one ion corresponds exactly to that seen in any other ion. That is, we assume that there is negligible proper motion between corresponding velocity components of all ionic species." Since an accuracy of  $2 \times 10^{-6}$  is claimed for the Many-Multiplet measurements, the above assumption implies that all ions have exactly the same velocity structure to better than  $1 \text{ km s}^{-1}$ . No such assumption is required for the O III method.

The Many-Multiplet assumption that all ions have the same velocity profile to better than  $1 \text{ km s}^{-1}$  may be testable directly by different groups using very high resolution absorption-line spectroscopy (resolution  $10^5$  or better) on relatively bright quasars. If the assumption of essentially identical line profiles is correct, one would expect that all absorption lines measured by the Many-Multiplet collaboration at a given redshift would be proportionally represented in all sub-clouds. Since absorption structures break up at high resolution into many clouds (see Bahcall 1975 or almost any modern high-resolution spectroscopic study of quasar absorption line spectra), one can compare the relative strengths of the Mg I, Mg II, Al II, Si II, Cr II, Fe II, Ni II, and Zn II lines in different sub-clouds. One might possibly be able to use the different measured line strengths to construct composite line profiles for different ions.

#### 8.2.5. *Line strengths, Misidentification, Blending*

We consider only strong O III emission lines, lines that can easily be recognized by a computer (or by a human eye) as having a high signal-to-noise ratio, at least 20:1 (see § 5.5). In our Standard Sample, the average (median) equivalent width of the 5007 Å line is 68 Å (57 Å). The Many-Multiplet method uses weak as well as strong lines.

There is no significant chance that the O III lines will be misidentified or strongly blended. There is no other pair of strong emission lines in the relevant part of quasar (or galaxy) spectra (Vanden Berk et al. 2001). We algorithmically exclude spectra in which the H $\beta$  line is sufficiently strong to possibly contaminate the measurement of the wavelengths of the 5007 Å and 4959 Å lines. For absorption line features, on the hand, there is a significant chance of blending, particularly for the crowded absorption line spectra that are observed at large redshifts.

Line identification is much more difficult for the Many-Multiplet method. The line identification codes are necessarily complicated and the logic of how different lines are identified depends, among other things, upon the signal-to-noise ratio of each spectrum, the richness of the absorption

line spectrum, the physical assumptions that one makes about the absorbers (e.g., chemical composition and ionization state), the assumed standard lines, the confidence level at which one makes the line identifications, the decision tree used when multiple identifications are possible (e.g., at different redshifts) for the same absorption lines, and the way one treats blending (for a discussion of some of these complications see, e.g., Bahcall 1968 and Bahcall et al. 1993, 1996).

#### 8.2.6. Full disclosure

All of the spectra we use in measuring the O III lines are available in the SDSS EDR (see Schneider et al. 2002). We describe in detail in § 2—§ 5 how our measurements were made. Table 5 lists all of the quasars that passed at least three of the four standard tests we have used.

Reduced spectra of the region around the O III emission lines are available publicly for all quasars that are included in our standard sample. The O III lines stand out clearly (to visual inspection or to algorithmic selection). The spectra can be down-loaded at <http://www.sns.ias.edu/~jnb>.

The situation is more complex for the Many-Multiplet method. Not all of the spectra are publicly available. The line identifications depend upon many assumptions (see discussion in § 8.2.5 and in Bahcall 1968 and Bahcall et al. 1993, 1996). One must decide whether a given set of lines is, e. g., Zn II at one redshift or a combination of lines from different ions at different redshifts. Using spectra taken over a large redshift range ( $0.2 < z < 3.7$ ) with different telescopes, full disclosure under these circumstances would be an enormous task. Consistent with this difficulty, the detailed reduced spectra have not made been made public by the Many-Multiplet collaboration and, for example, the justifications for the line identifications of less abundant ions like Cr II, Ni II, and Zn II are not given explicitly.

#### 8.2.7. Local value of $\alpha$

Finally, the results presented in this paper for the O III method are independent of the precise value of the fine structure constant at the present epoch. No assumption was made about the precise value of  $\alpha^2(0)$  in deriving the numerical constraints on the time dependence of  $\alpha$  that are presented in the first 16 rows (samples) of Table 1 and Table 2. The results given in the first 16 rows of the tables and in Eq. (21) depend only on measurements of the ratio of  $\alpha^2(t)/\alpha^2(0)$ . If one is only interested in whether or not  $\alpha^2(t)/\alpha^2(0)$  is time dependent, it does not matter what constant value one assumes for  $\alpha^2(0)$ . In this sense, the O III method is self-calibrating.

## 9. Discussion

We use the strong nebular lines of O III, 5007 Å and 4959 Å, to establish an upper limit to the time dependence of the fine structure constant,  $|\alpha^{-1}(d\alpha/dt)| < 10^{-13} \text{ yr}^{-1}$  [see Eq. (23)]. The limit is essentially the same for all 17 variations of the selection criteria for the sample that we have analyzed. The lack of a measurable time dependence can be seen visually in Figure 6. We have used spectra from the early data release sample (Schneider et al. 2002) of the Sloan Digital Sky Survey.

The reduced spectra for the 44 quasars in our standard sample are available publicly at the URL <http://www.sns.ias.edu/~jnb>. The O III lines stand out strongly in all spectra that we measure.

The upper limit derived here on the change of  $\alpha(t)$  over a characteristic time of  $4 \times 10^9 \text{ yr}$  [cf. Eq. (19)] is robust. We present in § 7 and in Table 1 and Table 2 results for 17 different algorithms for determining the average value, and the rate of change, of  $\alpha^2$  during the cosmic epoch explored. The results for all the samples we have considered are in agreement.

Depending upon the algorithm adopted for selecting the sample, the sample size varies from a minimum of 29 quasars to a maximum of 73 quasars, with 44 quasars in our Standard Sample (cf. Table 1 and Table 2). Essentially identical results are obtained if one uses a weighted or unweighted average of the measurements, adopts a more stringent restriction on the strength of possibly contaminating H $\beta$  emissions, relaxes the signal to noise requirement, omits or changes the way the Kolmogorov-Smirnov test is applied, omits each of the other three defining selection criteria, considers equivalent widths rather than area under the O III emission lines, removes the most distant outlier, compares measurements made for small and large redshifts, adopts an extreme cosmology, or includes the result for a local measurement of  $\alpha$ .

As a by-product of the measurements performed here, we derived in § 4.1 a precise value,  $3.01 \pm 0.02$ , for the ratio of the photon fluxes corresponding to the 5007 Å and the 4959 Å lines. Thus the ratio of the Einstein A coefficients for the two lines is  $A(5007)/A(4959) = 3.01 \pm 0.02$ . Our measured value for  $A(5007)/A(4959)$  is in good agreement with previous theoretical estimates, which provides some support for the validity of the measurements that we have made. However, our measurement of  $A(5007)/A(4959)$  is more accurate than the previous theoretical estimates.

Over the immense cosmic time interval explored using the [O III] emission lines, the fractional change in  $\alpha$  is small,  $\Delta\alpha/\alpha(0) = (-2 \pm 1.2) \times 10^{-4}$ . This null result is consistent with all the measurements that we know about from other methods (Savedoff 1956; Bahcall & Schmidt 1967; Bahcall, Sargent, & Schmidt 1967; Wolfe, Brown, & Roberts 1976; Levshakov 1994; Potekhin & Varshalovich 1994; Cowie & Songaila 1995; Ivanchik, Potekhin, & Varshalovich 1999; and Uzan 2002), including other measurements of quasar absorption line spectra and terrestrial laboratory measurements. Only the recent results that were obtained using the Many-Multiplet method suggest a non-zero time-dependence for  $\alpha$ ; the suggested rate of change is consistent with the previous and present null results for astronomical measurements. The Many-multiplet collaboration con-

cludes in published papers that  $\Delta\alpha/\alpha(0) = (-0.7 \pm 0.2) \times 10^{-5}$  over the redshift range of 0.5 to 3.5 (Murphy et al. 2001b; see also Dzuba, Flambaum, & Webb 1999a,b; Webb et al. 1999; Murphy et al. 2001a; and Webb et al. 2002).

Table 3 and § 8 compare the O III and the Many-Multiplet method. The O III method is simpler and less subject to systematic uncertainties, but the Many-Multiplet method has the advantage of greater potential precision since one considers many more transitions. As explained in § 8, the higher precision claimed for the Many-Multiplet method comes at a price, namely: 1) the necessity for detailed modeling of the line profiles from different clouds; 2) the measurement of absolute (instead of relative) wavelengths to a sample average accuracy of  $\sim 0.0002 \text{ \AA}$ ; 3) reliance on relativistic, many body calculations of the size of the  $\alpha^4$  contributions to atomic energy levels; and 4) the possible misidentification or blending of weak features. The Many-Multiplet assumption that the velocity profiles of different ions are the same to an accuracy of  $1 \text{ km s}^{-1}$  may be testable with independent very high-resolution spectra of relatively bright quasars (see discussion near the end of § 8.2.4).

The Many-Multiplet collaboration finds a small, non-zero but constant value for  $\Delta\alpha/\alpha(0)$  above redshifts of about unity. The effect reported by the Many-Multiplet collaboration is one and a half orders of magnitude smaller than the upper limit obtained in this paper using the Early Release SDSS data. We believe that, for the O III method, statistical errors dominate the uncertainty in the current measurements. We would like to improve the result given in this paper by using much larger quasar samples from the SDSS and 2dF surveys, when they become publicly available.

Does the fine-structure constant vary with cosmological epoch? After the extensive discussion given in this paper of measurements of the time dependence of  $\alpha$ , we would like to be able say something definitive to the reader about this question. However, nothing that we have said in this paper contradicts the claims by the Many-Multiplet collaboration to have measured a time-dependence at a level of sensitivity well below what is currently obtainable with the O III method. We have not found, nor even looked for, an error in the analysis of the Many-Multiplet collaboration. The best wisdom that we can offer the reader on the question of whether  $\alpha$  is time dependent is that the answer depends upon which Bayesian priors one adopts, a matter about which reasonable scientists can disagree. For example, which is *a priori* more probable: that  $\alpha$  is constant or that the velocity profiles of a variety of absorbing ions from a number of different absorbing clouds are the same and can be modeled correctly to an accuracy of  $1 \text{ km s}^{-1}$ ?

We are grateful to Dr. J. Reader, Group Leader of Atomic Spectroscopy at the National Institute of Standards and Technology, for valuable suggestions and advice. The reader will find useful related information at the NIST Atomic Spectra Database: [http://physics.nist.gov/cgi-bin/AtData/main\\_asd](http://physics.nist.gov/cgi-bin/AtData/main_asd). We are indebted to B. Draine and J. Schaye for valuable comments on a draft of this paper and to R. Lupton and M. Strauss for generous help with data reduction issues. We appreciate helpful email exchanges with V. Flambaum and J. Webb. JNB is supported in part

by a NSF grant #PHY-0070928.

### A. Is $R(t)$ proportional to $\alpha^2(t)$ ?

The principal assumption made in the text is that the difference in wavelengths divided by their sum is proportional to the fine-structure constant squared. For simplicity of description, we have proceeded as if the numerator of  $R(t)$  (see Eq. A4) were proportional to  $\alpha^4$  and the denominator was proportional to  $\alpha^2$ , so that their ratio was proportional to  $\alpha^2$ . In fact, we know that there are both  $\alpha^2$  and  $\alpha^4$  terms (non-relativistic and relativistic terms) in the denominator.

How do the presence of both  $\alpha^4$  and  $\alpha^2$  terms in the denominator of  $R(t)$  (cf. Eq. 1) affect the slope,  $S$  (cf. Eq. 7), which represents the linear time dependence of  $\alpha^2(t)$ ? We answer this question in this Appendix.

Let the shorter wavelength, higher frequency transition be denoted by  $\nu_1$ . Then we can write

$$\nu_1 = \nu_0 [1 + B_1 \alpha^2], \quad \nu_1 = \frac{c}{4959 \text{ \AA}}, \quad (\text{A1})$$

where  $\nu_0$  ( $\propto \alpha^2$ ) is the non-relativistic atomic energy difference and the relativistic terms, including the spin orbit interaction, are represented by  $B_1 \alpha^2$ . Similarly, for the longer wavelength, lower frequency transition we can write

$$\nu_2 = \nu_0 [1 + B_2 \alpha^2], \quad \nu_2 = \frac{c}{5007 \text{ \AA}}. \quad (\text{A2})$$

The measured fine-structure splitting,  $(\Delta\nu)_{\text{fine structure}}$ , satisfies the relation

$$(\Delta\nu)_{\text{fine structure}} \propto (B_1 - B_2) \alpha^2(t). \quad (\text{A3})$$

In principle, we could use relativistic Hartree-Fock calculations to estimate the values of  $B_1$  and  $B_2$ . We prefer not to use theoretical calculations that could have an unknown systematic error and instead rely upon measured wavelengths only. This empiricism results in a small ambiguity in the meaning of any time dependence that is ultimately measured. However, as we shall now show, this ambiguity is numerically unimportant.

The quantity we use to measure  $\alpha^2(t)/\alpha^2(0)$  is (cf. Eq. 1)

$$\frac{R(t)}{R(0)} = \left[ \frac{\lambda_2(t) - \lambda_1(t)}{\lambda_2(t) + \lambda_1(t)} \right] \left[ \frac{\lambda_2(0) + \lambda_1(0)}{\lambda_2(0) - \lambda_1(0)} \right]. \quad (\text{A4})$$

Substituting Eq. (A1) and Eq. (A2) into Eq. (A4) and carrying out the straightforward algebra, we find

$$\frac{R(t)}{R(0)} \cong \left[ 1 + StH_0 \left\{ 1 - \frac{(B_1 + B_2) \alpha^2(0)}{2} \right\} \right], \quad (\text{A5})$$

where the slope  $S$  is defined by Eq. (7). Let  $\Delta\nu$  be the energy difference corresponding to the wavelength splitting of 47.93 Å (cf. Figure 1). Then one can easily see that if  $\nu_2 < \nu_0 < \nu_1$ , then

$$\left| \frac{(B_1 + B_2) \alpha^2(0)}{2} \right| \sim \frac{\Delta\nu}{2\nu_0} \simeq 0.005. \quad (\text{A6})$$

If  $\nu_0$  does not satisfy the above inequality, then  $| (B_1 + B_2) \alpha^2(0)/2 |$  can be of order 0.01.

In all cases, the presence of both  $\alpha^2$  and  $\alpha^4$  terms in the denominator of  $R(t)$  only changes the interpretation of the slope  $S$  by a negligible amount. The next higher order terms in the atomic energies (or frequencies), which arise from the Lamb shift, change the interpretation of  $S$  by less than 1%.

## B. Data Tables

In this section, we present data tables that may be of interest to the specialist. Table 4 presents the measurements of  $\eta$  and  $A$ , and the inferred value of  $\alpha^2/\alpha^2(0)$ , for the Standard Sample of 44 quasars. Table 5 presents, for all 107 quasars that passed at least three of the four standard selection tests, the tests that each quasar passed and the measured values of  $\eta$  and  $A$ . Table 6 lists the SDSS name and an alternative catalog name for quasars we have studied that have been previously listed in other catalogs.

Table 4. Measurements for the Standard Sample. The table contains the quasar name (with an asterisk if previously discovered by another survey), the SDSS redshift, the measured value of  $\alpha^2$ , the relative displaced  $\eta$  of the 5007 Å and 4959 Å lines, and the relative scaling  $A$ , of the two lines. Quasars marked with an asterisk have an alternative catalog name listed in Table 6.

Quasar Name	$z$	$\alpha^2/\alpha^2(0)$	$\eta \times 10^3$	$A$
SDSS 000859+011351	0.28678	$1.0012 \pm 0.0026$	9.6775	2.80
SDSS 001030+010006	0.37792	$1.0015 \pm 0.0010$	9.6800	3.05
SDSS 001327+005231*	0.36219	$1.0021 \pm 0.0012$	9.6859	3.05
SDSS 001545+000822	0.37091	$1.0002 \pm 0.0013$	9.6681	3.14
SDSS 004458+004319	0.34979	$0.9983 \pm 0.0012$	9.6496	2.93
SDSS 005717+003242	0.49178	$0.9990 \pm 0.0015$	9.6564	2.95
SDSS 011420–004049	0.43913	$0.9969 \pm 0.0021$	9.6354	3.24
SDSS 012050–001832	0.34901	$0.9981 \pm 0.0026$	9.6478	2.95
SDSS 012750–000919	0.43766	$1.0005 \pm 0.0009$	9.6711	2.99
SDSS 013352+011345*	0.30804	$0.9987 \pm 0.0020$	9.6531	3.04
SDSS 015950+002340*	0.16313	$0.9967 \pm 0.0012$	9.6337	3.04
SDSS 020115+003135	0.36229	$0.9993 \pm 0.0017$	9.6586	3.05
SDSS 021259–003029	0.39449	$0.9999 \pm 0.0007$	9.6649	2.94
SDSS 021359+004226	0.18243	$0.9991 \pm 0.0006$	9.6572	2.83
SDSS 024706+002318	0.36322	$0.9980 \pm 0.0018$	9.6465	2.96
SDSS 025432–004220*	0.43390	$1.0019 \pm 0.0017$	9.6841	3.03
SDSS 030100+000429	0.48595	$0.9993 \pm 0.0019$	9.6589	3.15
SDSS 030335+004144	0.66911	$1.0004 \pm 0.0024$	9.6696	3.29
SDSS 032559+000800	0.36019	$0.9984 \pm 0.0019$	9.6503	2.89
SDSS 033202–003739	0.60729	$0.9997 \pm 0.0042$	9.6630	3.15
SDSS 095625–000353*	0.51217	$0.9997 \pm 0.0015$	9.6632	2.97
SDSS 102700–010424	0.34379	$0.9990 \pm 0.0009$	9.6558	3.02
SDSS 104132–005057	0.30281	$0.9986 \pm 0.0026$	9.6520	3.27
SDSS 105151–005117*	0.35892	$0.9993 \pm 0.0005$	9.6586	2.99
SDSS 105706–004145	0.18776	$0.9997 \pm 0.0030$	9.6626	3.12
SDSS 111353–000217	0.44544	$1.0009 \pm 0.0008$	9.6745	2.98
SDSS 114313+002937*	0.64159	$1.0024 \pm 0.0018$	9.6888	2.95
SDSS 115758–002220	0.25960	$1.0003 \pm 0.0006$	9.6683	2.95
SDSS 130713–003601	0.17012	$0.9994 \pm 0.0011$	9.6596	2.96
SDSS 134113–005315*	0.23745	$1.0006 \pm 0.0009$	9.6718	3.01
SDSS 134459–001559*	0.24475	$0.9981 \pm 0.0006$	9.6474	3.07
SDSS 134507–001900	0.41867	$0.9995 \pm 0.0010$	9.6614	3.05
SDSS 142648+005323	0.21956	$1.0003 \pm 0.0014$	9.6688	2.94

Table 4—Continued

Quasar Name	$z$	$\alpha^2/\alpha^2(0)$	$\eta \times 10^3$	$A$
SDSS 145221+002359	0.45792	$0.9954 \pm 0.0012$	9.6210	3.07
SDSS 153911+002600	0.26491	$1.0045 \pm 0.0032$	9.7100	2.84
SDSS 172032+551330	0.27235	$1.0006 \pm 0.0011$	9.6720	2.94
SDSS 172206+565451	0.42554	$1.0085 \pm 0.0029$	9.7481	2.79
SDSS 173311+535457	0.30721	$0.9990 \pm 0.0025$	9.6560	3.22
SDSS 232640–003041	0.58191	$1.0010 \pm 0.0030$	9.6760	3.08
SDSS 234145–004640	0.52386	$0.9991 \pm 0.0024$	9.6571	2.95
SDSS 235156–010913*	0.17407	$1.0015 \pm 0.0024$	9.6802	3.15
SDSS 235439+005751	0.38974	$0.9973 \pm 0.0017$	9.6398	2.82
SDSS 235441–000448	0.27877	$0.9926 \pm 0.0033$	9.5937	2.72
SDSS 235732–002845	0.50829	$0.9992 \pm 0.0026$	9.6576	2.95

Table 5. Results for 107 quasars. Table 5 includes all SDSS EDR quasars that passed at least three of the four standard tests described in § 5. The table shows which of the four tests the quasar passed. The tests (a)-(d), refer, respectively to the KS test, lining up the peaks of the two [O III] emission lines, the H $\beta$  contamination, and the signal to noise ratio of the lines. The quantity  $\eta$  is defined by Eq. (15) and  $A$  is the ratio of the intensity of the 5007 Å line to the intensity of the 4959 Å line. Quasars marked with an asterisk have an alternative catalog name listed in Table 6.

Quasars	$z$	Tests	$\eta \times 10^{+3}$	$A$
SDSS 000859+011351	0.287	(a)(b)(c)(d)	9.677	2.80
SDSS 001030+010006	0.378	(a)(b)(c)(d)	9.680	3.05
SDSS 001327+005231*	0.362	(a)(b)(c)(d)	9.686	3.05
SDSS 001545+000822	0.371	(a)(b)(c)(d)	9.668	3.14
SDSS 002311+003517*	0.422	(a) (c)(d)	9.633	2.84
SDSS 002444+003221*	0.402	(b)(c)(d)	9.667	2.82
SDSS 003242+003110	0.361	(a)(b)(c)	9.627	3.23
SDSS 003431–001312	0.381	(b)(c)(d)	9.677	3.16
SDSS 004458+004319	0.350	(a)(b)(c)(d)	9.650	2.93
SDSS 005717+003242	0.492	(a)(b)(c)(d)	9.656	2.95
SDSS 011420–004049	0.439	(a)(b)(c)(d)	9.635	3.24
SDSS 012050–001832	0.349	(a)(b)(c)(d)	9.648	2.95
SDSS 012750–000919	0.438	(a)(b)(c)(d)	9.671	2.99
SDSS 013352+011345*	0.308	(a)(b)(c)(d)	9.653	3.04
SDSS 014017–005002*	0.334	(a)(b)(c)	9.669	3.15
SDSS 015629+000724	0.360	(a)(b) (d)	9.668	2.79
SDSS 015950+002340*	0.163	(a)(b)(c)(d)	9.634	3.04
SDSS 020115+003135	0.362	(a)(b)(c)(d)	9.659	3.05
SDSS 021225+010056	0.513	(b)(c)(d)	9.636	3.02
SDSS 021259–003029	0.394	(a)(b)(c)(d)	9.665	2.94
SDSS 021359+004226	0.182	(a)(b)(c)(d)	9.657	2.83
SDSS 021652–002335	0.305	(b)(c)(d)	9.702	2.94
SDSS 022119+005628	0.400	(a) (c)(d)	9.622	2.86
SDSS 022259–005035	0.553	(a)(b) (d)	9.625	3.01
SDSS 024651–005931*	0.468	(a)(b)(c)	9.688	2.90
SDSS 024706+002318	0.363	(a)(b)(c)(d)	9.647	2.96
SDSS 024954+010148*	0.585	(b)(c)(d)	9.714	2.86
SDSS 025007+002525*	0.197	(a)(b)(c)	9.672	2.93
SDSS 025432–004220*	0.434	(a)(b)(c)(d)	9.684	3.03
SDSS 025646+011349	0.177	(b)(c)(d)	9.663	3.05
SDSS 025735–001631	0.362	(a)(b) (d)	9.671	3.72
SDSS 030048+005440*	0.662	(a)(b)(c)(d)	9.625	2.70
SDSS 030100+000429	0.486	(a)(b)(c)(d)	9.659	3.15

Table 5—Continued

Quasars	$z$	Tests	$\eta \times 10^{+3}$	A
SDSS 030313–001457*	0.700	(b)(c)(d)	9.784	2.89
SDSS 030335+004144	0.669	(a)(b)(c)(d)	9.670	3.29
SDSS 031226–003709	0.621	(b)(c)(d)	9.651	2.99
SDSS 032559+000800	0.360	(a)(b)(c)(d)	9.650	2.89
SDSS 032628–002741	0.445	(b)(c)(d)	9.678	2.43
SDSS 033032–001743	0.609	(a)(b)(d)	9.473	2.65
SDSS 033202–003739	0.607	(a)(b)(c)(d)	9.663	3.15
SDSS 033606–000754	0.432	(b)(c)(d)	9.670	3.14
SDSS 034106+004610	0.634	(b)(c)(d)	9.659	2.71
SDSS 034247+010932	0.360	(b)(c)(d)	9.687	3.03
SDSS 034345–004801	0.746	(a)(c)(d)	9.613	3.17
SDSS 095625–000353*	0.512	(a)(b)(c)(d)	9.663	2.97
SDSS 101044+004331*	0.178	(a)(b)(c)	9.642	3.09
SDSS 102502+003126*	0.363	(b)(c)(d)	9.812	3.19
SDSS 102700–010424	0.344	(a)(b)(c)(d)	9.656	3.02
SDSS 104132–005057	0.303	(a)(b)(c)(d)	9.652	3.27
SDSS 105151–005117*	0.359	(a)(b)(c)(d)	9.659	2.99
SDSS 105228–010448	0.435	(b)(c)(d)	9.678	3.01
SDSS 105337+005958	0.476	(b)(c)(d)	9.643	3.05
SDSS 105706–004145	0.188	(a)(b)(c)(d)	9.663	3.12
SDSS 105935–000551	0.282	(a)(b)(c)	9.695	3.50
SDSS 111231–002534	0.544	(b)(c)(d)	9.677	3.04
SDSS 111353–000217	0.445	(a)(b)(c)(d)	9.674	2.98
SDSS 114313+002937*	0.642	(a)(b)(c)(d)	9.689	2.95
SDSS 115758–002220	0.260	(a)(b)(c)(d)	9.668	2.95
SDSS 120620–003852*	0.566	(b)(c)(d)	9.659	3.25
SDSS 122004–002539*	0.421	(b)(c)(d)	9.666	2.95
SDSS 125607+000207*	0.651	(a)(b)(c)	9.650	3.38
SDSS 130002–010601	0.307	(a)(b)(c)(d)	9.660	3.01
SDSS 130713–003601	0.170	(a)(b)(c)(d)	9.660	2.96
SDSS 132748–001021*	0.479	(b)(c)(d)	9.690	2.93
SDSS 134113–005315*	0.237	(a)(b)(c)(d)	9.672	3.01
SDSS 134251–005345*	0.326	(b)(c)(d)	9.279	3.67

Table 5—Continued

Quasars	$z$	Tests	$\eta \times 10^{+3}$	A
SDSS 134459–001559*	0.245	(a)(b)(c)(d)	9.647	3.07
SDSS 134507–001900	0.419	(a)(b)(c)(d)	9.661	3.05
SDSS 135553+001137	0.460	(b)(c)(d)	9.660	2.95
SDSS 135726+001542	0.661	(b)(c)(d)	9.667	2.80
SDSS 140827+004815	0.442	(b)(c)(d)	9.659	3.17
SDSS 140926–001415	0.468	(a) (c)(d)	9.636	3.02
SDSS 141637+003352*	0.434	(a) (c)(d)	9.644	3.03
SDSS 142648+005323	0.220	(a)(b)(c)(d)	9.669	2.94
SDSS 145221+002359	0.458	(a)(b)(c)(d)	9.621	3.07
SDSS 150629+003543	0.370	(b)(c)(d)	9.682	2.98
SDSS 151722–003002	0.445	(a)(b)(c)(d)	9.422	3.98
SDSS 152110+000304	0.465	(a) (c)(d)	9.656	3.13
SDSS 153306+000635	0.589	(b)(c)(d)	9.715	2.99
SDSS 153911+002600	0.265	(a)(b)(c)(d)	9.710	2.84
SDSS 165627+623226	0.185	(a) (c)(d)	9.615	2.89
SDSS 170956+573225	0.522	(a)(b)(c)	9.680	3.04
SDSS 171441+644155*	0.285	(a)(b)(c)	9.679	3.23
SDSS 171902+593715	0.178	(a)(b)(c)	9.638	2.98
SDSS 172032+551330	0.272	(a)(b)(c)(d)	9.672	2.94
SDSS 172059+612811	0.236	(b)(c)(d)	9.655	3.21
SDSS 172206+565451	0.426	(a)(b)(c)(d)	9.748	2.79
SDSS 172446+575453	0.676	(a)(b) (d)	9.586	3.11
SDSS 172543+580604	0.292	(b)(c)(d)	9.649	2.88
SDSS 172554+562458	0.736	(a)(b) (d)	9.634	2.71
SDSS 173229+564811	0.303	(a)(b)(c)	9.657	2.77
SDSS 173311+535457	0.307	(a)(b)(c)(d)	9.656	3.22
SDSS 173602+554040	0.497	(b)(c)(d)	9.677	2.83
SDSS 173638+535432	0.408	(b)(c)(d)	9.662	3.21
SDSS 173641+543350	0.551	(a)(b)(c)	9.875	3.06
SDSS 173721+550321	0.333	(a)(b) (d)	9.667	2.82
SDSS 232307+011121	0.339	(a)(b)(c)	9.676	3.45
SDSS 232640–003041	0.582	(a)(b)(c)(d)	9.676	3.08
SDSS 232801+001705	0.411	(b)(c)(d)	9.649	3.02

Table 5—Continued

Quasars	$z$	Tests	$\eta \times 10^{+3}$	A
SDSS 233129–004933	0.615	(a) (c)(d)	9.670	3.28
SDSS 233517+010307	0.624	(a)(b) (d)	9.716	2.68
SDSS 234145–004640	0.524	(a)(b)(c)(d)	9.657	2.95
SDSS 235156–010913*	0.174	(a)(b)(c)(d)	9.680	3.15
SDSS 235409–001947*	0.461	(a) (c)(d)	9.697	2.84
SDSS 235439+005751	0.390	(a)(b)(c)(d)	9.640	2.82
SDSS 235441–000448	0.279	(a)(b)(c)(d)	9.594	2.72
SDSS 235732–002845	0.508	(a)(b)(c)(d)	9.658	2.95

Table 6. Alternative names. The table lists the SDSS name and an alternative catalog name for the 107 SDSS quasars that passed at least three of the four standard tests described in § 5 and that have been previously listed in other catalogs.

SDSS Name	Alternative Name
SDSS 001327+005231	LBQS 0010+0035
SDSS 002311+003517	LBQS 0020+0018
SDSS 002444+003221	LBQS 0022+0015
SDSS 013352+011345	UM 338
SDSS 014017–005002	UM 357
SDSS 015950+002340	MRK 1014
SDSS 024651–005931	[HB89] 0244–012
SDSS 024954+010148	US 3213
SDSS 025007+002525	LEDA 138544
SDSS 025432–004220	LBQS 0251–0054
SDSS 030048+005440	US 3513
SDSS 030313–001457	[HB89] 0300–004
SDSS 095625–000353	2QZ J095625.8–000354
SDSS 101044+004331	[VCV96] Q 1008+0058
SDSS 102502+003126	LBQS 1022+0046
SDSS 105151–005117	PG 1049–005
SDSS 114313+002937	2QZ J114313.4+002937
SDSS 120620–003852	2QZ J120620.5–003853
SDSS 122004–002539	2QZ J122004.3–002540
SDSS 125607+000207	2QZ J125607.8+000207
SDSS 132748–001021	2QZ J132748.1–001021
SDSS 134113–005315	LBQS 1338–0038
SDSS 134251–005345	LBQS 1340–0038
SDSS 134459–001559	LBQS 1342–0000
SDSS 141637+003352	2QZ J141637.4+003351
SDSS 171441+644155	HS 1714+6445
SDSS 235156–010913	[HB89] 2349–014
SDSS 235409–001947	LBQS 2351–0036

## REFERENCES

Bahcall, J. N., & Salpeter, E. E. 1965, *ApJ*, 142, L1677

Bahcall, J. N., Sargent, W. L. W., & Schmidt, M. 1967, *ApJ*, 149, L11

Bahcall, J. N., & Schmidt, M. 1967, *Phys. Rev. Lett.*, 19, 1294

Bahcall, J. N. 1968, *ApJ* 153, 679

Bahcall, J. N. 1975, *ApJ* 200, L1

Bahcall, J. N., et al. (the HST quasar absorption line Key Project collaboration) 1993, *ApJS* 87, 1

Bahcall, J. N., et al. (the HST quasar absorption line Key Project collaboration) 1996, *ApJ* 457, 19

Boyle, B. J., Shanks, T., Croom, S. M., Smith, R. J., Miller, L., Loaring, N., & Heymans, C. 2000, *MNRAS*, 317, 1014

Burles, S. and Schlegel, D. 2003, in preparation

Carroll, S. M., & Press, W. H. 1992, *ARA&A*, 30, 499

Cowie, L. L., & Songaila, A. 1995, *ApJ*, 453, 596

Croom, S. M., Smith, R. J., Boyle, B. J., Shanks, T., Loaring, N. S., Miller, L., & Lewis, I. J. 2001, *MNRAS*, 322, L29

Dzuba, V. A., Flambaum, V. V., & Webb, J. K. 1999a, *Phys. Rev. A*, 59, 230

Dzuba, V. A., Flambaum, V. V., & Webb, J. K. 1999b, *Phys. Rev. Lett.*, 82, 888

Freedman, W. L., et al. 2001, *ApJ* 553, 47

Ivanchik, A. V., Potekhin, A. Y., & Varshalovich, D. A. 1999, *A&A*, 343, 439

Levshakov, S. A. 1994, *MNRAS*, 269, 339

Marciano, W. J. 1984, *Phys. Rev. Lett.*, 52, 489

Moorwood, A. F. M., Salinari, P., Furniss, I., Jennings, R. E., & King, K. J. 1980, *A&A*, 90, 304

Murphy, M. T., Webb, J. K., Flambaum, V. V., Churchill, C. W., & Prochaska, J. X. 2001a, *MNRAS*, 327, 1223

Murphy, M. T., Webb, J. K., Flambaum, V. V., Dzuba, V. A., Churchill, C. w., Prochaska, J. X., Barrow, J. D., & Wolfe, A. M. 2001b, *MNRAS*, 327, 1208

Pettersson, S.-G. 1982, *Physica Scripta*, 26, 296

Peck, E. R., & Reeder, K. 1972, *J. Opt. Soc. Am.*, 62, 958

Potekhim, A. Y., & Varshalovich, D. A. 1994, *A&A Supl. Ser.*, 104, 89

Savedoff, M. P. 1956, *Nature (London)*, 176, 688

Schlegel, D. 2003, in preparation

Schneider, D. P., et al. 2002, *AJ*, 123, 567

Stoughton, C., et al. 2002, *AJ*, 123, 485

Uzan, J.-P. 2002, *Rev. Mod. Phys.*, in press (hep-ph/0205340)

Vanden Berk, D. E., et al. 2001, *AJ*, 122, 549

Webb, J. K., Flambaum, V. V., Churchill, C. W., Drinkwater, M. J., & Barrow, J. D. 1999, *Phys. Rev. Lett.*, 82, 884

Webb, J. K., Murphy, M. T., Flambaum, V. V., Dzuba, V. A., Barrow, J. D., Churchill, C. W., Prochaska, J. X., & Wolfe, A. M. 2002, *Phys. Rev. Lett.*, 87, 091301

Webb, J. K., Murphy, M. T., Flambaum, V., and Curran, S. J., in press (astro-ph/0210531)

Wiese, W. L., Fuhr, J. R., & Deters, T. R. 1996, *J. Phys. Chem. Ref. Data Monograph No. 7*

Wolfe, A. M., Brown, R. L., & Roberts, M. S. 1976, *Phys. Rev. Lett.*, 37, 179